Selection 6

Chaos, Solitons & Fractals Vol. 1, No. 3, pp.199–231, 1991
Printed in Great Britain

0960-0779/91$3.00 + 00
Pergamon Press plc

Survey of Regular and Chaotic Phenomena in the Forced Duffing Oscillator

YOSHISUKE UEDA

Department of Electrical Engineering, Kyoto University, Kyoto 606, Japan

(*Received* 11 *March* 1991)

Abstract—The periodically forced Duffing oscillator

$$\ddot{x} + k\dot{x} + x^3 = B\cos t$$

exhibits a wide variety of interesting phenomena which are fundamental to the behavior of nonlinear dynamical systems, such as regular and chaotic motions, coexisting attractors, regular and fractal basin boundaries, and local and global bifurcations. Analog and digital simulation experiments have provided a survey of the most significant types of behavior; these experiments are essential to any complete understanding, but the experiments alone are not sufficient, and careful interpretation in terms of the geometric theory of dynamical systems is required. The results of the author's survey, begun over 25 yr ago, are here brought together to give a reasonably complete view of the behavior of this important and prototypical dynamical system.

1. INTRODUCTION

Various fascinating and fundamental phenomena occur in nonlinear systems. One of the most representative and the simplest nonlinear systems may be the damped, periodically forced nonlinear oscillator governed by

$$\frac{d^2x}{dt^2} + k\frac{dx}{dt} + f(x) = e(t) \tag{1}$$

where k is a damping coefficient, $f(x)$ is a nonlinear restoring term and $e(t)$ is a periodic function of period T. This equation, first introduced by Duffing [1], has been studied both theoretically and experimentally by many researchers. From the phenomenological point of view, a steady state governed by Duffing's equation (1) may be a periodic motion, the fundamental period of which is either the period T of the external force, or its integral multiple. In more general dynamical systems, a steady state may be an almost periodic motion; however in the case of equation (1), the positive damping k eliminates this possibility [2]. Therefore, for the system under consideration, the regular motions are the periodic steady states. Regular motions have been extensively studied for more than 50 years. However, due to the completely deterministic nature of the equation, the possibility of chaotic motions was overlooked for a long time. The characteristic property of chaotic motion is that its long-term behavior cannot be reproduced in repeated trials from apparently identical initial condition. This contrasts dramatically with the perfect short-term predictability which is guaranteed by the deterministic nature of equation (1).

Even until the beginning of the 1970s, a prejudice existed that there can occur only two kinds of steady states in the second-order nonautonomous periodic systems, that is, periodic and almost periodic motions. A similar prejudice existed among physicists who conjectured that fluid turbulence is a complex form of almost periodic motion. This belief

was sharply challenged in 1971 by Ruelle and Takens, who suggested that irregular motions governed by strange attractors are a more likely explanation of turbulence [3]. In fact, the author had already observed an abundance of irregular behavior in second-order systems by this time, reported in [4]; this work achieved wider recognition through Professor Ruelle's articles in *La Recherche* and *The Mathematical Intelligencer* [5, 6], and later in the book of Thompson and Stewart [2].

The following Sections 2–5 contain some mathematical preliminaries [2, 7–16]; Section 2 is essential, but on first reading, Sections 3–5 may be skipped. Sections 6–8 present the results of analog and digital simulations and their interpretation.

2. STROBOSCOPIC OBSERVATION OF THE PHENOMENON: A BRIEF INTRODUCTION TO DISCRETE DYNAMICAL SYSTEMS THEORY [2, 8, 11–17]

Before entering into particular results for the Duffing oscillator, let us briefly explain the fundamental concepts of discrete dynamical systems theory in relation to nonlinear differential equations of the second order.

The equation (1) is a particular case of a nonautonomous periodic system,

$$\frac{dx}{dt} = X(t, x, y), \qquad \frac{dy}{dt} = Y(t, x, y) \tag{2}$$

where $X(t, x, y)$ and $Y(t, x, y)$ are both periodic in t with period T. Here sufficient continuity properties of X and Y are assumed to guarantee the existence and the uniqueness of solutions for any initial condition and for all $t \geqq t_0$.

A solution of equation (2) determines a motion of a representative point on the xy plane. Let us consider the solution

$$x = x(t;\ t_0, x_0, y_0), \qquad y = y(t;\ t_0, x_0, y_0) \tag{3}$$

of equation (2) which when $t = t_0$ is at the arbitrary point $p_0(x_0, y_0)$ of the xy plane. The solution (3) describes a curve in the txy space, and the projection of this solution curve on the xy plane represents the phase-plane trajectory of the motion starting from p_0 at $t = t_0$. Let us focus our attention on the location of the representative point $p_n(x_n, y_n)$ at the instant $t = t_0 + nT$, n being 0, 1, 2, ... An infinite point sequence

$$\{p_0, p_1, p_2, \ldots\} \tag{4}$$

where $x_n = x(t_0 + nT;\ t_0, x_0, y_0)$, $y_n = y(t_0 + nT;\ t_0, x_0, y_0)$ is called a positive half-sequence or half-orbit of p_0. This half-orbit represents the behavior of the motion starting from p_0, that is, as time proceeds, or as n tends to infinity, the point p_n approaches, through the transient state, the set of points which represents steady final motion. An accumulation point of the positive half-orbit (4) of p_0 is called an ω-limit point and a set of such points is called an ω-limit set of p_0. An α-limit point and an α-limit set of p_0 are also defined, with reference to a negative half-orbit with $n = 0, -1, -2, \ldots,$. An orbit is a negative half orbit to p_0 plus the positive half-orbit from p_0. An orbit together with its α- and ω-limit sets is called a complete group.

This stroboscopic observation is illustrated in Fig. 1 by putting $t_0 = 0$. The constant t_0 represents the phase of the stroboscopic observation and it can be any chosen value between 0 and T. The choice of t_0 may change the locations of stroboscopic points of the orbit but does not alter their topological structure. Also it should be noted that due to the periodicity of X and Y the translation of the time axis by an arbitrary multiple of T does not alter the situation.

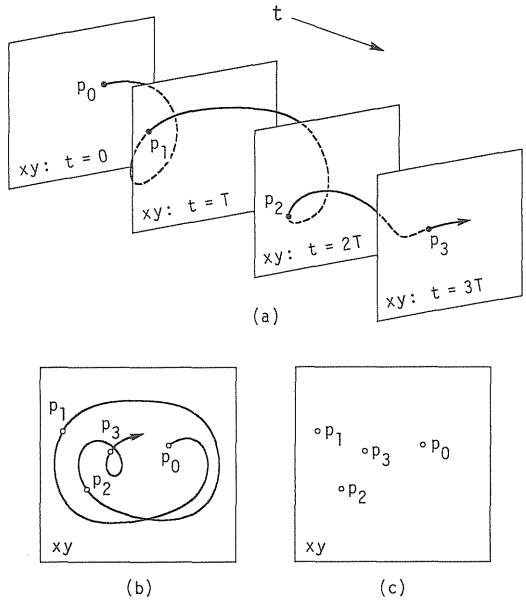

Fig. 1. Schematic illustration of stroboscopic observation. (a) Solution curve in the *txy* space; (b) trajectory projected onto the *xy* plane; (c) stroboscopic positive half-orbit in the *xy* plane.

This stroboscopic observation of the phenomenon can be stated in terms of discrete dynamical systems theory. The solution of equation (2) defines a discrete dynamical system on $\mathbf{R}^2$, or a mapping of the *xy* plane into itself,

$$\left.\begin{aligned} f_\lambda\colon\ & \mathbf{R}^2 \to \mathbf{R}^2 \\ & p_0 \mapsto p_1 \end{aligned}\right\} \tag{5}$$

where $p_1 = f_\lambda(p_0)$ is an image of p_0 under the mapping and λ denotes a set of parameters contained in X and Y of equation (2). We also write the inverse mapping by $p_0 = f_\lambda^{-1}(p_1)$, and nth iterations of the mapping by $p_n = f_\lambda^n(p_0)$. From the properties of the solutions of differential equations, it is known that the mapping (5) is a homeomorphism, that is, a one-to-one continuous mapping with a continuous inverse. Under sufficient smoothness assumptions, this mapping is a diffeomorphism, that is, the mapping and its inverse have continuous derivatives. Finally, the mapping (5) is always orientation-preserving.

By applying the mapping thus introduced to investigate the behaviour of the solution curves in the *txy* space, we have only to study the successive images of initial points in the *xy* plane, or the discrete dynamical system in the *xy* plane into itself. If a solution $(x(t), y(t))$ has period T, then the point $p_0(x(0), y(0))$ is a fixed point of the mapping f_λ. This situation is illustrated in Fig. 2. If a solution has period mT, that is, a solution of period mT but not of period less than mT, the points $p_1, p_2, \ldots, p_m$ are all fixed points of the mapping f_λ^m. Each point is called an m-periodic point, and the totality of these points is called an m-periodic group. This situation is illustrated in Fig. 3 for $m = 2$.

By identifying $t = 0$ with $t = T$, the equation (2) can be transformed to a phase space which is the Cartesian product of the *xy* plane with the circle representing periodic time.

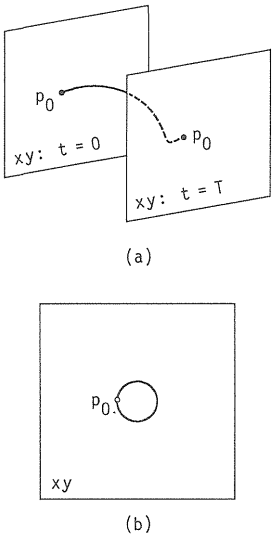

Fig. 2. Periodic solution with period T and fixed point p_0.

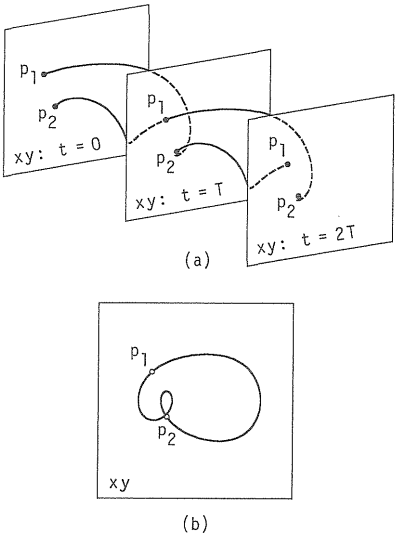

Fig. 3. Periodic solution with period $2T$ and two-periodic points p_1 and p_2.

This shows that the stroboscopic map f_λ is an example of a Poincaré map, and the stroboscopic orbit is a Poincaré section of the solution curve in txy space.

3. MAXIMAL BOUNDED INVARIANT SET AND CENTRAL MOTIONS [8, 17–19]

Under rather general conditions satisfied in practice, there exist simple closed curves in the xy plane such that a solution of equation (2) can intersect any one of these curves only by crossing it from the domain exterior to the curve into the domain interior to the curve. Moreover, a curve with this property can be constructed in such a manner that it passes through any point in the xy plane sufficiently remote from the origin and encircles the origin of the xy plane. Therefore a curve Γ_0 can be found such that all solutions starting outside Γ_0 must eventually pass through Γ_0 to the interior and remain inside for all subsequent time.

If Γ_0 denotes a simple closed curve of this type, it follows that under iterations of the mapping f_λ all points exterior to Γ_0 are transferred into interior points. In practice we may choose Γ_0 such that the interior Δ_0 of Γ_0 is mapped under one iteration to the domain Δ_1 interior to $\Gamma_1 = f_\lambda(\Gamma_0)$. If $f_\lambda^n(\Gamma_0)$ is denoted by Γ_n and the closed domain bounded by Γ_n in the xy plane by Δ_n, then Δ_n lies in the domain interior to Δ_{n-1}, that is, $\Delta_n \subset \Delta_{n-1}$ holds.

The closed set

$$\Delta = \bigcap_{n=0}^{\infty} \Delta_n \tag{6}$$

is called the maximal bounded invariant set.

A similar construction was given by Levinson for a class of systems (2) which are dissipative at large displacements, or class D; he showed that the maximal bounded

invariant set so constructed is closed, connected, and has the property that images of a point which is not contained in Δ tend to Δ under iterations of the mapping f_λ. This invariant set Δ contains all the dynamics of the steady states in the system (2), however, it contains points representing not only steady states but also some transient states.

Let us introduce the concepts of non-wandering set and central motions introduced by G. D. Birkhoff. It was Birkhoff who first investigated the comprehensive mathematical description of steady states in nonlinear systems. Consider an arbitrary connected region σ on the xy plane. It may happen that σ is intersected by none of its images

$$\ldots, \sigma_{-2}, \sigma_{-1}, \sigma_1, \sigma_2, \ldots \tag{7}$$

where $\sigma_n = f_\lambda^n(\sigma)$, in which case σ is called a wandering region and its points wandering points. Obviously, wandering points represent transient states; let us denote the totality of wandering points of the xy plane by W^1. A point in the xy plane which is contained in no wandering region is called a non-wandering point. The totality of non-wandering points of the xy plane constitutes a non-empty closed invariant set M^1 towards which all other points of Δ tend asymptotically on indefinite iteration of f_λ or f_λ^{-1}.

Let us suppose now that M^1 is not identical with Δ, and let us take the set M^1 as fundamental instead of Δ. A connected region which contains points of M^1 will be called wandering with respect to M^1 if the set $\sigma \cap M^1$ of points common to σ and M^1 is intersected by none of its images under powers of f_λ or f_λ^{-1}. The points of M^1 which are contained in such a region are called wandering with respect to M^1, and their totality is denoted by W^2. The set $M^2 = M^1 - W^2$ consists of the points which are non-wandering with respect to M^1. In the case where $M^1 = M^2$, M^1 is called non-wandering with respect to itself.

In principle this construction can be repeated; Birkhoff composed a sequence

$$M^1, M^2, M^3, \ldots \tag{8}$$

where each set is non-empty and a proper subset of all those preceding it. He proved that this sequence terminates with $M^r = M^{r+1} = \ldots$ which therefore must be non-wandering with respect to itself. The points of M^r are called central points, and motions started from central points are called central motions.

In the 1960s, C. Pugh proved a remarkable theorem, the so-called closing lemma, which has a corollary that in a generic system the periodic orbits are dense in the non-wandering set M^1 [20]. Hence every point in M^1 is non-wandering with respect to M^1, and M^1 is equal to the set of central motions. Although numerical studies by their nature cannot confirm this mathematical theorem, we may say that extensive numerical experience reveals no contradiction to Pugh's results.

Here let us decompose a set of central points. A point which is both an α- and ω-limit point is called pseudo-recurrent. The characteristic property of such a point is that it returns infinitely often into an arbitrary small neighborhood of itself under indefinite iteration of f_λ as well as f_λ^{-1}. Birkhoff proved that the set of central points consists of the pseudo-recurrent points together with their derived set, a central point is either a pseudo-recurrent point or an accumulation point of pseudo-recurrent points. The complete group of a pseudo-recurrent point is called a quasi-minimal set.

If a non-empty invariant closed set in a quasi-minimal set is identical with the quasi-minimal set itself, the quasi-minimal set is called a minimal set, and points of a minimal set are called recurrent points. Obviously, an orbit of a recurrent point, or the minimal set itself represents a single final motion or the smallest unit of a theoretical or an ideal steady state.

4. FIXED AND PERIODIC POINTS AND RELATED PROPERTIES [17, 21]

Let us consider the classification of fixed and periodic points according to the type and the number of these points contained in the maximal bounded invariant set Δ. These are the simplest type of minimal sets among the solutions of equation (2). The behavior of successive images in the neighborhood of a fixed or a periodic point determines the stability of the associated periodic solution. Let $p_0(x_0, y_0)$ be a fixed point and $q_0(x_0 + \xi_0, y_0 + \eta_0)$ be a neighboring point of p_0. Let $q_1(x_0 + \xi_1, y_0 + \eta_1)$ be an image of q_0 under the mapping f_λ, then the following relation results

$$\left.\begin{aligned} x_0 + \xi_1 &= x(t_0 + T;\ t_0,\ x_0 + \xi_0,\ y_0 + \eta_0) \\ y_0 + \eta_1 &= y(t_0 + T;\ t_0,\ x_0 + \xi_0,\ y_0 + \eta_0) \end{aligned}\right\} . \tag{9}$$

This situation is illustrated in Fig. 4(a) with $t_0 = 0$. As shown in the figure, when q_0 is varied to encircle p_0, its image q_1 traces out an ellipse around p_0 in the same sense as q_0. For small values of ξ_0 and η_0, ξ_1 and η_1 can be expanded into power series in ξ_0 and η_0,

$$\left.\begin{aligned} \xi_1 &= a\xi_0 + b\eta_0 + \dots \\ \eta_1 &= c\xi_0 + d\eta_0 + \dots \end{aligned}\right\} \tag{10}$$

with $a = (\partial x/\partial \xi_0)_0$, $b = (\partial x/\partial \eta_0)_0$, $c = (\partial y/\partial \xi_0)_0$ and $d = (\partial y/\partial \eta_0)_0$ where $(*)_0$ denotes the value of $(*)$ at $\xi_0 = \eta_0 = 0$. The terms not explicitly given in the right-hand side of equation (10) are of degree higher than the first in ξ_0 and η_0. Equation (10) describes the mapping $q_0 \mapsto q_1$ in the neighborhood of the fixed point p_0, and this mapping is characterized by the roots ρ_1 and ρ_2 of the equation,

$$\begin{vmatrix} a - \rho & b \\ c & d - \rho \end{vmatrix} = 0. \tag{11}$$

Since the roots ρ_1 and ρ_2 are determined from the quadratic equation, they are either both real or else are conjugate complex. However, in this case, from the general theory of differential equations, their product is always positive, because the following relation holds,

$$\begin{vmatrix} a & b \\ c & d \end{vmatrix} = \exp\left[\int_{t_0}^{t_0+T} \left(\frac{\partial X}{\partial x} + \frac{\partial Y}{\partial y}\right)_0 \mathrm{d}t\right] \tag{12}$$

where $(*)_0$ denotes the value of $(*)$ at the periodic solution under consideration.

The fixed point p_0 is called simple if both $|\rho_1|$ and $|\rho_2|$ are different from unity. If one or both $|\rho_1|$ and $|\rho_2|$ is unity, this means that the fixed point is multiple. Levinson classified simple fixed points as follows:

sink or completely stable if	$\lvert\rho_1\rvert < 1,\ \lvert\rho_2\rvert < 1$
source or completely unstable if	$\lvert\rho_1\rvert > 1,\ \lvert\rho_2\rvert > 1$
saddle or directly unstable if	$0 < \rho_2 < 1 < \rho_1$
saddle or inversely unstable if	$\rho_2 < -1 < \rho_1 < 0.$

The same classification also applies to periodic points.

If a fixed point is a sink, there is a neighborhood of the fixed point which contracts to the point as shown in Fig. 4(a) and (b); all points in this neighborhood tend to the fixed point under repeated application of the mapping f_λ. This implies that as t tends to infinity, the corresponding solutions tend to the periodic solution, so that this periodic solution is asymptotically stable in the sense of Lyapunov. If a fixed point is a source, a neighborhood

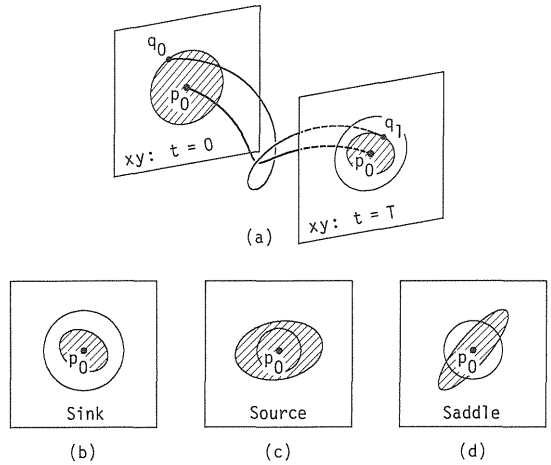

Fig. 4. Behavior of images in the neighborhood of a periodic solution according to stability type of the fixed point. (a) Schematic txy diagram; (b) sink; (c) source; (d) saddle.

of the fixed point expands from the point as shown in Fig. 4(c) and all points in this neighborhood move away from the fixed point under the mapping f_λ. If a fixed point is a saddle, we have the situation of a neighborhood which expands and contracts locally under the mapping f_λ as shown in Fig. 4(d). In this case, there abut at the saddle four invariant curves or branches: two α-branches, whose points converge toward the saddle on iteration of f_λ^{-1}, and two ω-branches, whose points converge toward the saddle on iteration of f_λ. For the saddle, the difference between the directly and inversely unstable cases is illustrated in Fig. 5. Here successive locations of a periodic solution of equation (2) through one period are shown corresponding to a directly unstable fixed point D and an inversely unstable point I. By choosing the strobing angle at 12 different values progressing from 0 to T, we follow the rotation, expansion and contraction of the local α- and ω-branches. Note that for purpose of illustration, the phase plane at $t = T$ is slightly shifted from its position at $t = 0$, so that the final image of D (or I) may be distinguished from the initial image. In each case, the circular dot identifies an expanding α-branch and the square dot a contracting ω-branch. In the case of D, there is one full rotation during the period 0–T, while in the case of I there is a half-rotation over the period. This is only the simplest case; in general, D might make an integer number of rotations during one period, and I might make a half-integer number of rotations. Only the local linear portion of the α- and ω-branches are shown; larger portions would exhibit curvature due to nonlinearity.

Levinson and Massera have discussed the number of fixed points and periodic points of equation (2) in the xy plane. Let $N(n)$ be the total number of n-periodic points and $C(n)$ the total number of completely stable and completely unstable n-periodic points. Similarly, let $D(n)$ and $I(n)$ be the number of directly unstable and inversely unstable n-periodic points, respectively. When equation (2) has a maximal bounded invariant set and all periodic points are simple, we have the following.

For $n = 1$,

$$\left.\begin{aligned} C(1) + I(1) &= D(1) + 1, \\ N(1) &= 2D(1) + 1 \end{aligned}\right\}. \tag{13}$$

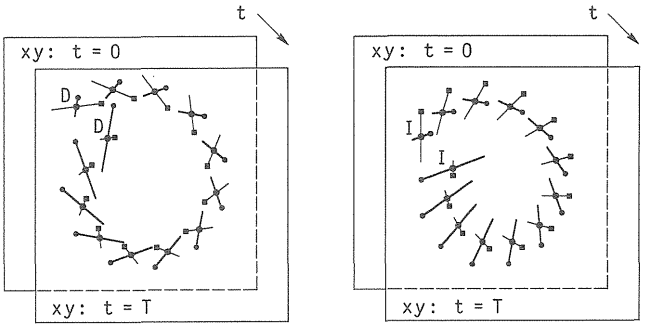

Fig. 5. Schematic diagram illustrating the difference between the two types of saddles. (a) Directly unstable saddle; (b) inversely unstable saddle.

For $n = 2, 4, 6, \ldots,$

$$\left.\begin{aligned} C(n) + I(n) &= D(n) + 2I(n/2), \\ N(n) &= 2[D(n) + I(n/2)] \end{aligned}\right\}. \tag{14}$$

For $n = 3, 5, 7, \ldots,$

$$\left.\begin{aligned} C(n) + I(n) &= D(n), \\ N(n) &= 2D(n) \end{aligned}\right\}. \tag{15}$$

These relations give an independent verification of whether a numerical search for fixed points or periodic points is complete. If the number and type of points observed do not conform to these relations, then undoubtedly there are additional points to be located; but of course the converse need not be true: the relations might be satisfied for a partial set of fixed and periodic points.

After the fixed and periodic points, the next simplest type of minimal set is an invariant closed curve in the stroboscopic or Poincaré section. As noted above, this phenomena cannot occur in a system with uniformly positive damping, so we shall not discuss it further here, and instead refer the reader to [17].

5. DOUBLY ASYMPTOTIC POINTS AND RELATED PROPERTIES [7, 8]

In systems described by autonomous differential equations of the second order, no two trajectories in the xy plane can intersect each other, and they may only approach each other asymptotically at the equilibrium points. However, in nonautonomous periodic systems of the second order, a somewhat different situation occurs: invariant branches of saddle points of the mapping f_λ^n may intersect one another, introducing a complicated structure into the dynamics. Here let us introduce some terminology and concepts defined by Poincaré, which describe this complexity.

We have already explained the α- and ω-branches of the saddles of the mapping f_λ^n. If we consider the totality of α- and ω-branches of fixed or periodic points of all orders in the

xy plane, it is readily shown that no α- (or ω-) branch can intersect another α- (or ω-) branch. However, an α-branch may intersect an ω-branch, and the points of intersection in such a case are called doubly asymptotic points.

A doubly asymptotic point is called homoclinic if the α- and ω-branches on which it lies issue from the same point or from two points belonging to the same periodic group. A homoclinic point of the former type is called simple. A doubly asymptotic point is called heteroclinic if the α- and ω-branches on which it lies issue from two periodic points, each of them belonging to different periodic groups. Also a doubly asymptotic point is said to be of general type if the two branches which intersect at the doubly asymptotic point cross transversely, that is, are not coincident or merely tangent at the point; in the contrary case the point is of special type. When a mapping has no doubly asymptotic points of special type and no fixed or periodic points of multiple type, the mapping is said to belong to the general analytic case.

Birkhoff proved the following theorems.

In the general analytic case, an arbitrary small neighborhood of a homoclinic point contains infinitely many periodic points.

In the general analytic case, an arbitrary small neighborhood of a homoclinic point contains a homoclinic point of simple type.

In order to illustrate these situations, Fig. 6 shows an example of a homoclinic point of simple type, together with sketches of portions of the α-branch (thick line) and the ω-branch (fine line). The existence of a homoclinic point H implies the existence of additional homoclinic points H_1, H_2, H_3, ..., and indeed an infinite sequence of homoclinic points approaching D along its ω-branch, each point being the image of its predecessor under f_λ. Likewise, successive pre-images H_{-1}, H_{-2} and so on are homoclinic points approaching D along its α-branch. Near D, the stretching and contraction of a neighborhood of H is governed by the local linear approximation of f_λ; the images of such a neighborhood, which are schematically shown by shaded regions, become extremely long and thin under iteration of f_λ near D. An example of a periodic point with images p_1, p_2, p_3, p_4, p_5, p_6 is indicated; additional periodic points of longer period lie nearer to the homoclinic points.

The original terms α- and ω-branch have been retained for reasons of nostalgia; in current parlance, the α-branch is called the unstable manifold, while the ω-branch is called the stable manifold. Another alternative and perhaps more suggestive terminology was proposed by Zeeman, who calls the α-branch the outset and the ω-branch the inset [22].

Up to this point, we have considered a mathematical description of behavior of an ideal dynamical system which is perfectly deterministic, not subject to any noise or disturbance, and described with total precision.

In what follows, we will investigate the behavior of this ideal system through real-world simulations using analog and digital computing devices. This brings unavoidable additional influences such as small amounts of noise, imperfect precision, and numerical errors due to approximate solution algorithms and roundoff. Although it may not be easy to incorporate these effects into rigorous mathematical analysis, these features of real-world simulations have a healthy influence in guiding our attention to the aspects of the invariant set which correspond to robust and stable behavior.

6. COLLECTION OF STEADY STATES IN THE DUFFING OSCILLATOR [23, 24]

As a specific example of equation (2), let us consider the Duffing equation

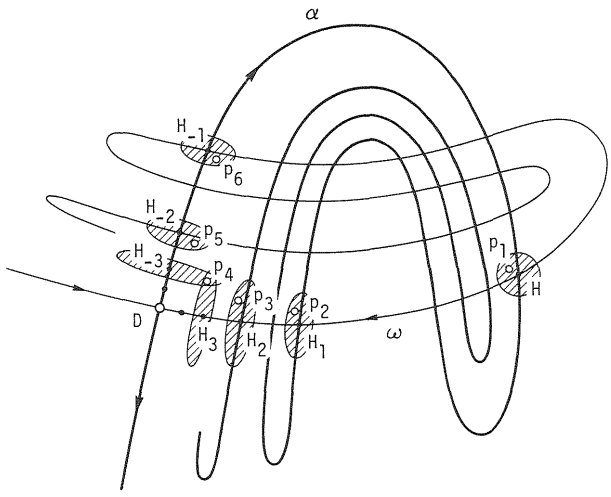

Fig. 6. Schematic illustration of a homoclinic structure, showing homoclinic points and neighboring periodic points.

$$\frac{d^2x}{dt^2} + k\frac{dx}{dt} + x^3 = B\cos t \tag{16}$$

or

$$\frac{dx}{dt} = y, \qquad \frac{dy}{dt} = -ky - x^3 + B\cos t. \tag{17}$$

This equation represents forced oscillations in a variety of applications, with constant positive damping coefficient k, and nonlinear restoring force x^3 representing the simplest form of hardening symmetric spring in a mechanical system, or of magnetic saturation in an electrical circuit with a saturable core inductor [25–27]. In the derivation of such an equation, some approximations and simplifying assumptions are introduced, and small fluctuations and noise are neglected.

One might also consider an apparently more general system with angular forcing frequency ω different from one and coefficient of x^3 different from one. However, such a system can always be brought to the form (16) by appropriately rescaling x and t. Although there are advantages to considering forcing frequency ω as a parameter, we use k and B as the coordinates of parameter space, and do not explicitly consider transformation to other equivalent parameter space coordinates such as ω and B.

The symmetry of equation (17), associated with its invariance under the substitution $-x \to x$, $-y \to y$, $t + \pi \to t$, implies that a periodic trajectory is either symmetric to itself with respect to the origin of the xy plane or it coexists with another periodic trajectory symmetric to it with respect to the origin. Note however that the stroboscopic points of symmetrically related trajectories will not appear to be symmetric unless one of the pair is strobed with phase shift π. Also the positive damping k results in the non-existence of sources and of invariant closed curves representing almost periodic motions; and the area of the maximal bounded invariant set Δ of the mapping f_λ defined by equation (17) is necessarily zero.

In the damped, forced oscillatory system given by equation (16), various types of steady states are observed depending on the system parameters $\lambda = (k, B)$ as well as on the initial conditions. Figure 7 shows the regions on the kB plane in which different steady motions

are observed. The regions are obtained by both analog and digital simulations. The roman numerals I, II, II′, III and IV characterize periodic motions with period 2π. The fractions m/n ($m = 1, 3, 4, 5, 6, 7, 11$ and $n = 2, 3$) indicate the regions in which subharmonic or ultrasubharmonic motions of order m/n occur. An ultrasubharmonic motion of order m/n is a periodic motion of period $2n\pi$, and whose principal frequency is m/n times the frequency of the external force. In addition to these regular steady states, chaotic motions take place in the shaded regions. In the area hatched by solid lines, chaotic motion occurs uniquely, independent of initial condition; while in the area hatched by broken lines, two different steady states coexist, one being chaotic and the other a regular motion. Which one occurs depends on the initial condition. Ultrasubharmonic motions of higher orders ($n = 4, 5, \ldots,$) can occur naturally in the system, but they exist only in narrow regions and are therefore omitted in Fig. 7. Also some subtle details of region boundaries are not represented.

In order to clarify the meaning of this kB chart, we choose a set of typical parameters $\lambda = (k, B)$ from each region. Their locations are indicated by letters from a to u in Fig. 7. Figure 8 shows the steady states trajectories observed at each of these 21 parameter values. In the figure we can see multiple steady states for certain parameter values. On the trajectories, a $\times$ marks the location of a stroboscopic point at the instant $t = 2i\pi$ (i being integer). Therefore these $\times$ marks show the sinks of the mapping f_λ^n ($n = 1, 2, 3$) in all cases where the attractor is a regular periodic motion, that is, all cases except (k), (l_1) and (o_1).

The three cases (k), (l_1) and (o_1) show chaotic motions in which the trajectories are drawn after the transient states have died away. The remarkable feature of the chaotic steady states is that, however small simulation error may be, the precise long-term trajectory cannot be reproduced in repeated experiments; but nevertheless the same structure always eventually develops. This is seen most clearly by stroboscopic sampling. To see the situation more clearly, only one trajectory was computed for a long time and its steady state stroboscopic orbit is shown in Fig. 9 for these three cases. The orbits thus obtained indicate the presence of chaotic attractors, that is, steady state motions with definite structure and also an aspect of randomness. Figure 10 shows corresponding waveforms obtained by analog simulation, which may be impossible to distinguish from outcomes of a random process.

As shown above multiple attractors are common in the system (17) and indeed there may be regular and chaotic attractors coexisting, for example, for the cases (l) and (o). Here we would like to associate each attractor with the ensemble of all starting points that settle to it; this point set is called its basin of attraction. These basins are separated by ω-branches of some saddle points in the xy plane, and together the basins of all attractors and their separators (basin boundaries) constitute the entire xy plane.

Figure 11 shows attractor-basin phase portraits at successive times differing by phase $\pi/6$, for the parameter values (o). In this case the maximal bounded invariant set consists of the following: a sink (circle), a directly unstable saddle (filled circle) together with its α-branches, and a chaotic attractor. The non-wandering set M^1 is the sink, saddle and chaotic attractor. In the sequence shown, one folding and stretching action is completed, and in the interval from $t = \pi$ to $t = 2\pi$ a second, symmetrically related folding and stretching is accomplished. As will be seen later, the chaotic attractor contains exactly three saddle fixed points, one of directly unstable type and two of inversely unstable type.

Here, let us proceed to the statistical time series analysis for a chaotic attractor. To this end, we regard the chaotic motion $\{X(t)\}$ as a periodic process $\{X_T(t)\}$ with a sufficiently long period T, where T is a multiple of 2π. Note that in this section only, we use T exclusively to stand for this very long observation interval, and not in the previous meaning

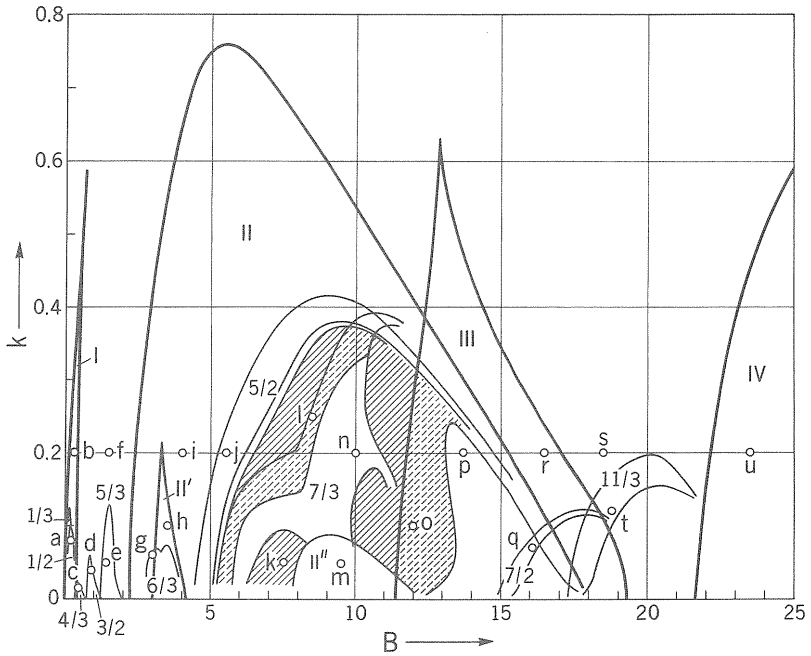

Fig. 7. Regions of different steady states for the system defined by equation (16). (Reproduced with the courtesy of the Society for Industrial and Applied Mathematics [24].)

of the period of the system, which is here taken equal to 2π.

Now suppose $x_T(t)$ to be a periodic function with period T, which coincides with a realization $x_T(t)$ of $\{X_T(t)\}$ in the interval $(-T/2, T/2]$. Then the realization $x_T(t)$ is expanded into Fourier series as

$$x_T(t) = \frac{a_0}{2} + \sum_{m=1}^{\infty} (a_m \cos m\omega_0 t + b_m \sin m\omega_0 t), \qquad \omega_0 = \frac{2\pi}{T} \tag{18}$$

where

$$\left.\begin{aligned} a_m &= \frac{2}{T}\int_{-T/2}^{T/2} x_T(t)\cos m\omega_0 t\,\mathrm{d}t \\ b_m &= \frac{2}{T}\int_{-T/2}^{T/2} x_T(t)\sin m\omega_0 t\,\mathrm{d}t \\ m &= 0, 1, 2, \ldots. \end{aligned}\right\} \tag{19}$$

Fourier coefficients a_m and b_m can not be distinguished from random variables because $x_T(t)$ is a sample function of the process $\{X_T(t)\}$. From these coefficients, the mean value $m_X(t)$ and the average power spectrum $\Phi_X(\omega)$ of the process $\{X(t)\}$ can be estimated as follows.

$$m_X(t) = \langle X(t)\rangle = \lim_{T\to\infty} \langle X_T(t)\rangle$$

$$\fallingdotseq \langle X_T(t)\rangle = \left\langle \frac{a_0}{2}\right\rangle + \sum_{m=1}^{\infty} [\langle a_m\rangle \cos m\omega_0 t + \langle b_m\rangle \sin m\omega_0 t] \tag{20}$$

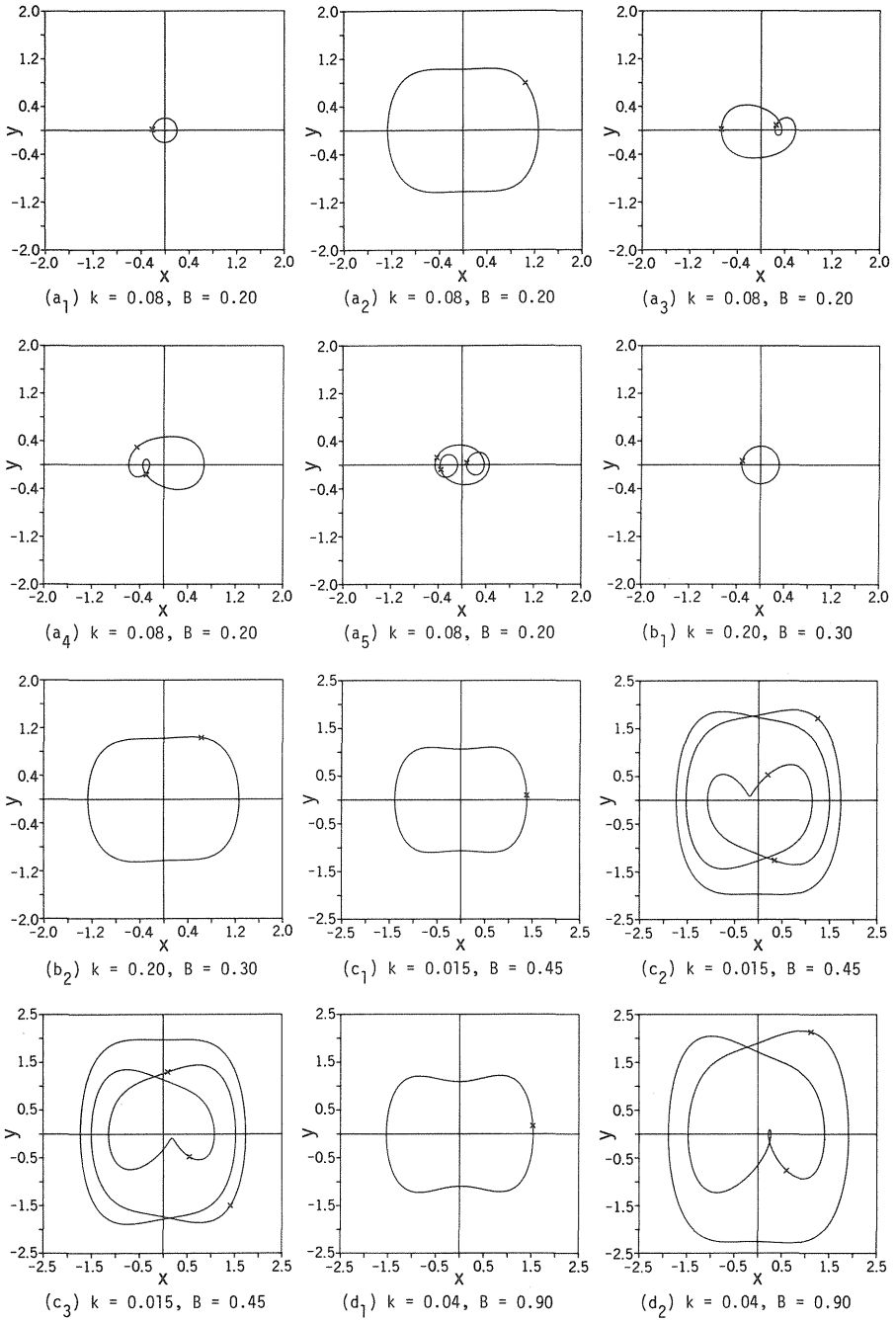

Fig. 8. continued on p. 212.

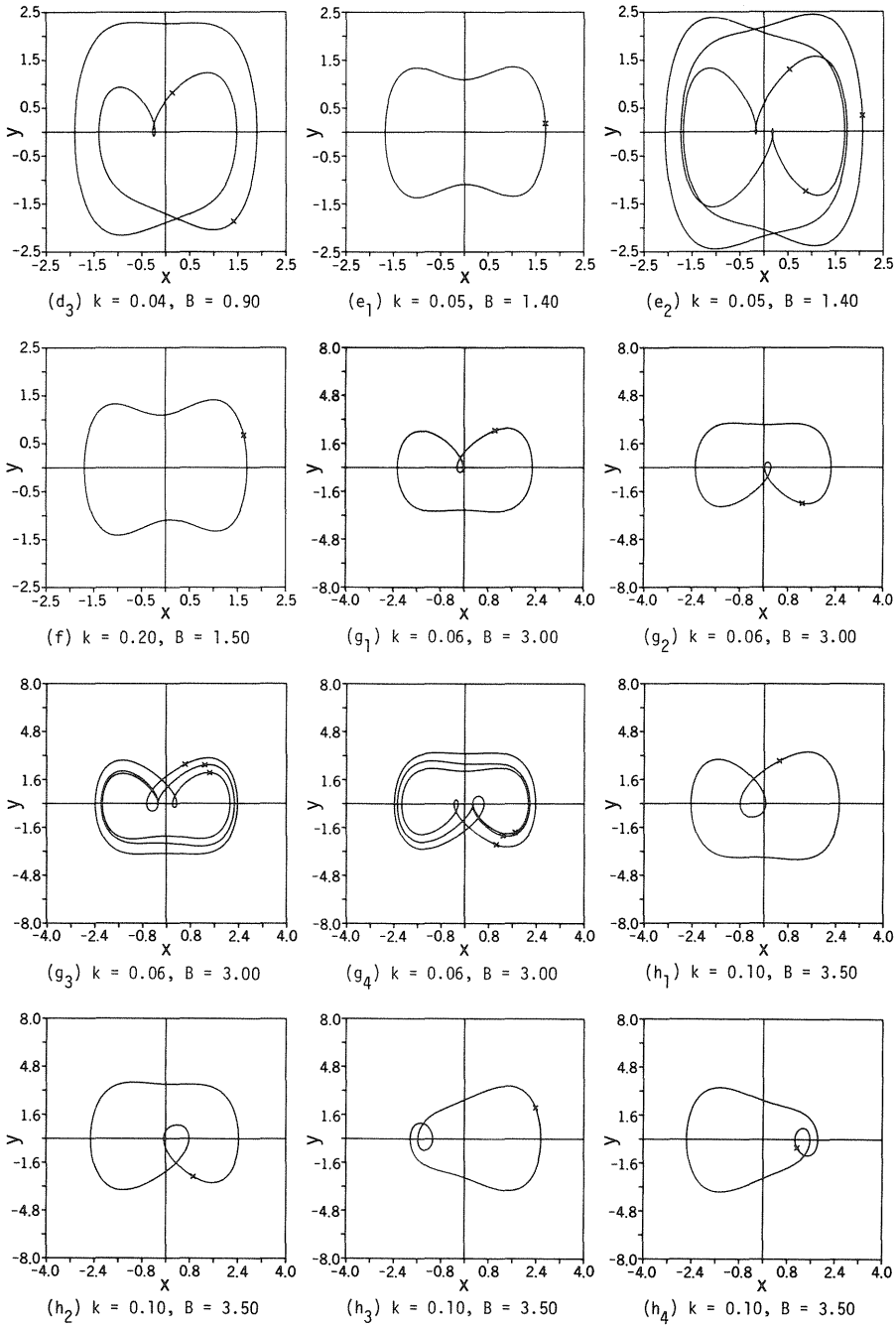

Fig. 8. continued on p. 213.

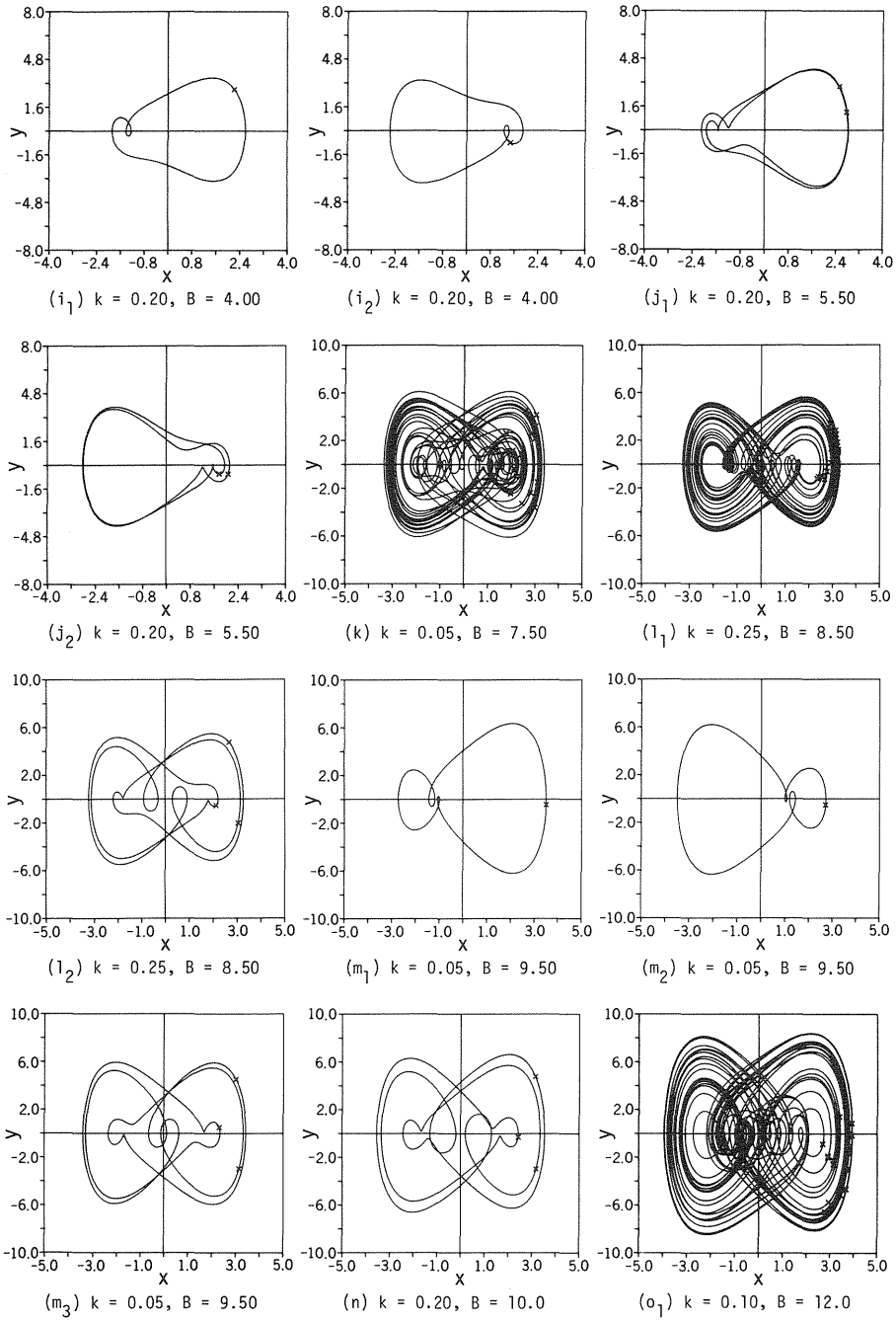

Fig. 8. continued on p. 214.

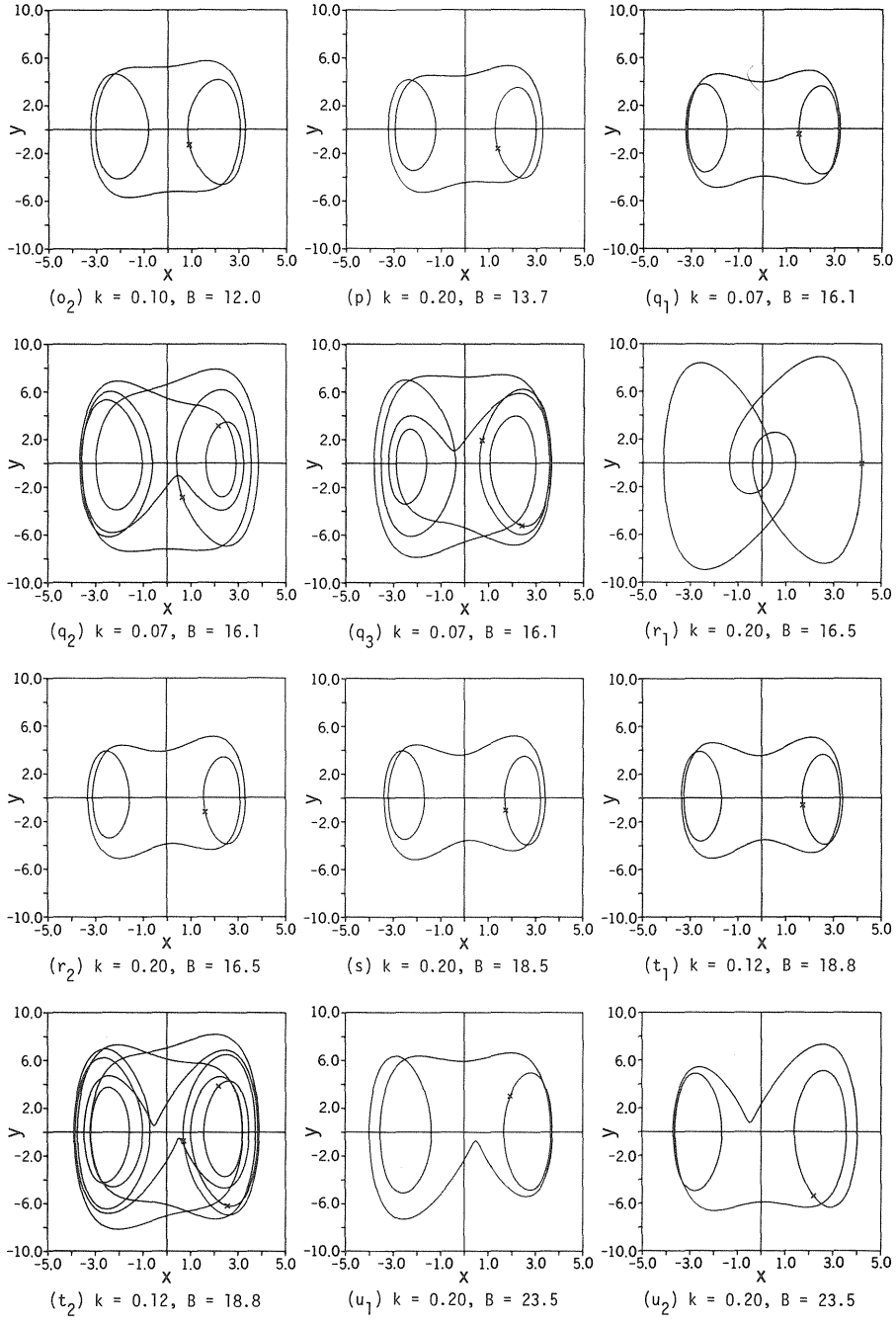

Fig. 8. Trajectories of various types of steady motion. (Reproduced with the courtesy of the Society for Industrial and Applied Mathematics [24].)

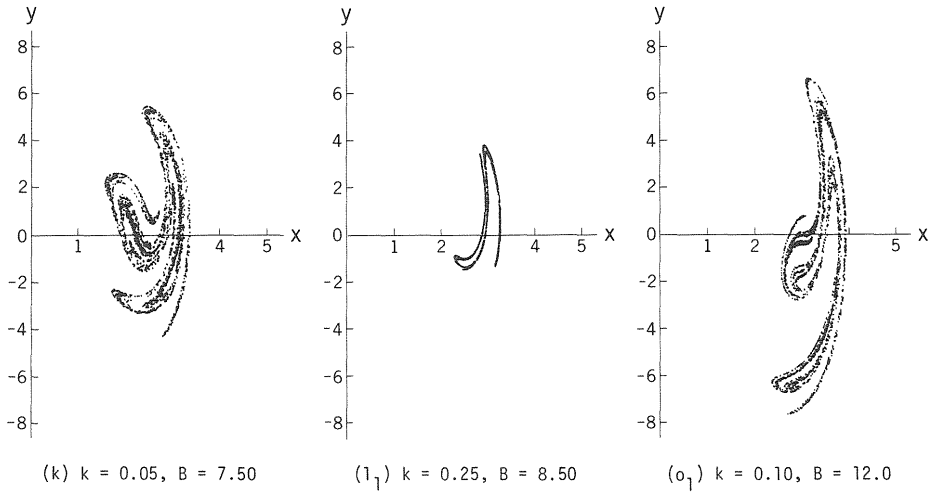

Fig. 9. Chaotic attractors for three representative sets of parameter values. (Reproduced with the courtesy of the Society for Industrial and Applied Mathematics [24].)

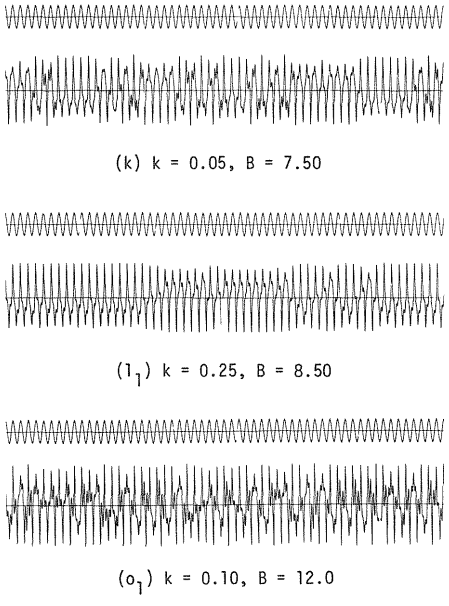

Fig. 10. Waveforms corresponding to the chaotic attractors of Fig. 9 obtained by analog simulation. (Reproduced with the courtesy of the Society for Industrial and Applied Mathematics [24].)

$$\Phi_X(\omega) = \lim_{T\to\infty} \left\langle \frac{1}{T} \left| \int_{-T/2}^{T/2} x_T(t) e^{-i\omega t}\, dt \right|^2 \right\rangle$$

$$\doteq \Phi_X(m\omega_0) = \frac{2\pi}{\omega_0} \left\langle \frac{1}{4}(a_m^2 + b_m^2) \right\rangle, \quad \omega_0 = \frac{2\pi}{T}. \tag{21}$$

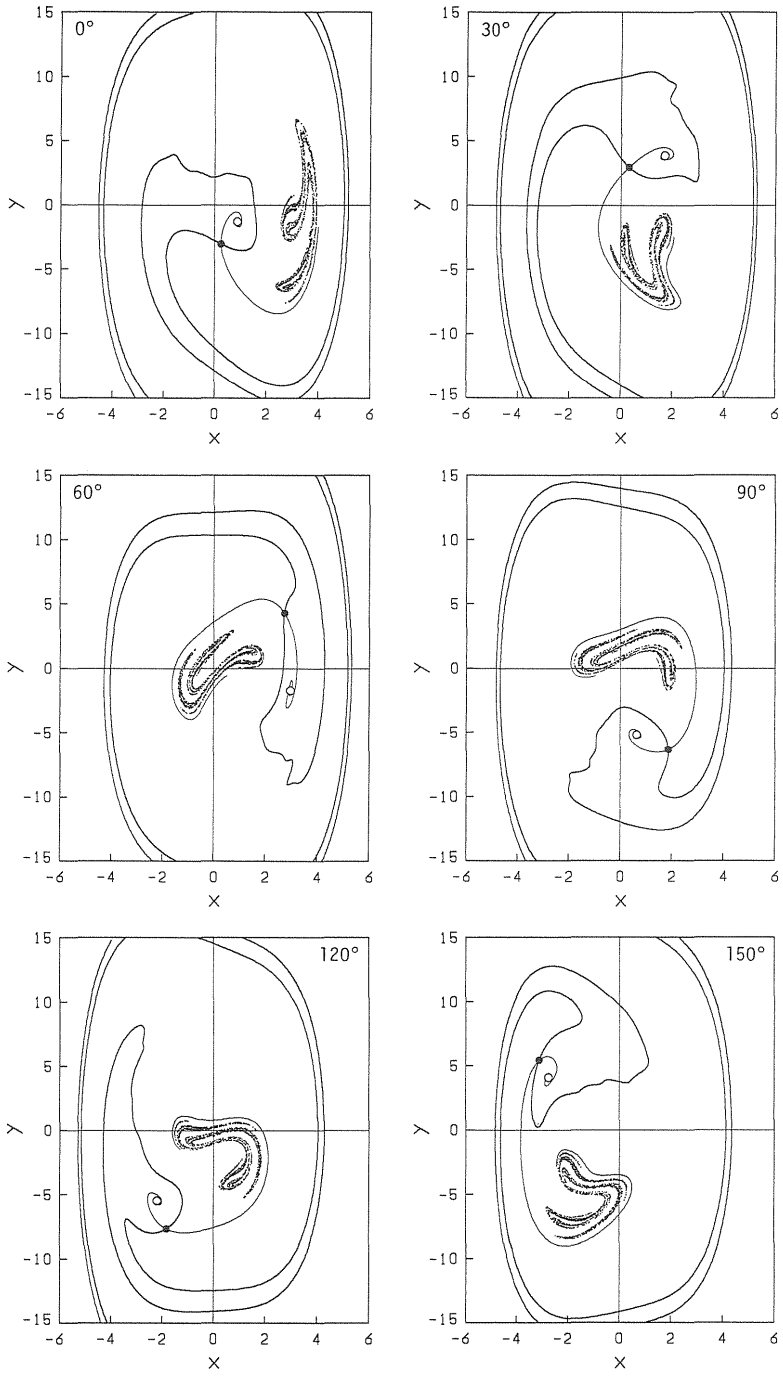

Fig. 11. Attractor-basin phase portraits at successive times differing by phase $\pi/6$ at the parameters (o) of Fig. 7 showing folding and stretching action.

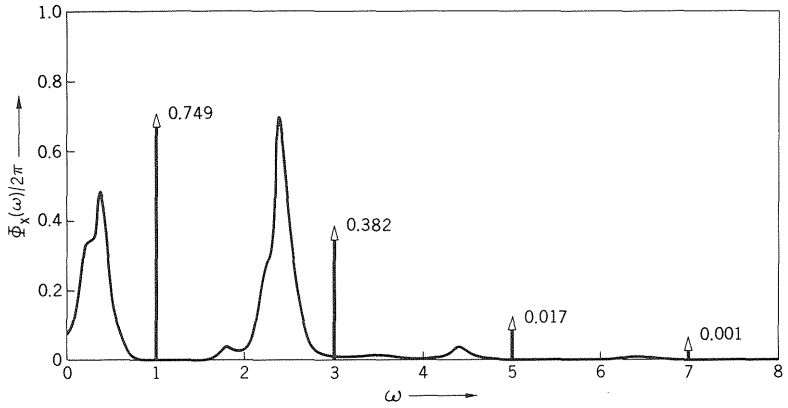

Fig. 12. Average power spectrum of the chaotic motion corresponding to the chaotic attractor of Fig. $9(o_1)$. (Reproduced with the courtesy of the Institute of Electrical Engineers of Japan [23].)

The ensemble average can be calculated by regarding successive waveforms in the intervals $((n - 1/2)T, (n + 1/2)T]$, $(n = 0, 1, 2, \ldots, N_S)$ as sample functions of $\{X_T(t)\}$.

Let us give an example thus estimated for the representative case of the system parameters (o), that is, $\lambda = (k, B) = (0.1, 12.0)$. The mean value of $\{X(t)\}$ was computed by Fast Fourier Transforms of numerical solutions over observation intervals $T = 2\pi \times 2^{10}$ with 100 samples, and was found to be

$$\begin{aligned} m_X(t) = {} & 1.72\cos t + 0.22\sin t \\ & + 1.21\cos 3t - 0.26\sin 3t \\ & + 0.25\cos 5t - 0.06\sin 5t \\ & + 0.07\cos 7t - 0.02\sin 7t \\ & + 0.02\cos 9t - 0.01\sin 9t. \end{aligned} \tag{22}$$

The mean value is found to be a periodic function. This indicates that the process $\{X(t)\}$ is a periodic non-stationary process. Figure 12 shows the average power spectrum estimated by using equation (21). In the figure, line spectra at $\omega = 1, 3, 5, \ldots$, indicate the periodic components of the mean value as given by equation (22), and numerical values attached to line spectra represent the power concentrated at those frequencies. Besides the line spectra, there are continuous power spectra representing the chaotic component. The average power of this process $\{X(t)\}$ is given by

$$\lim_{T\to\infty} \frac{1}{T} \int_{-T/2}^{T/2} \langle X_T^2(t) \rangle \, \mathrm{d}t \fallingdotseq \frac{1}{T} \int_{-T/2}^{T/2} \langle X_T^2(t) \rangle \, \mathrm{d}t = 3.08. \tag{23}$$

By adding noise in the numerical integration scheme, we have also confirmed that chaotic attractors as well as averages and spectra of the corresponding chaotic motions are insensitive to numerical error or noise in the computer experiment. Therefore, it was conjectured that the average power spectrum of the process is a characteristic of the global structure of the chaotic attractor, independent of the nature of small uncertain factors or microfluctuations in the actual systems.

7. COLLECTION OF ATTRACTOR-BASIN PHASE PORTRAITS [28]

A typical example of an attractor-basin phase portrait was shown in the preceding section as the stroboscopic Poincaré section at various phases. In these portraits, basin boundaries were given by ω-branches of saddles of the mapping f_λ in the xy plane. These boundaries were located by tracing ω-branches from the saddles by reversing time in the simulation. For the example given in Fig. 11, ω-branches were rather simple and smooth, hence they were located with fairly good accuracy. However, as will be seen later, for the case of fractal basin boundaries, it becomes very difficult with this method of analysis to locate the basin boundaries, because ω-branches become infinitely stretched and folded by homoclinic structure, therefore we cannot avoid considerable error in locating fine details of tangled basin boundaries by numerical experiment. In these situations, the full complexity of basin boundaries must be identified by exhaustive trial of various starting conditions.

In order to supplement the preceding collection of steady states, let us here survey attractor-basin phase portraits for additional representative sets of system parameters $\lambda = (k, B)$. Figures 13 and 14 illustrate the difference between smooth and fractal basin boundaries. In both cases, there are two attractors (sinks) represented by small circles; the shaded regions show the basins of attraction of the resonant motions, while the blank regions represent non-resonant ones. There exist directly unstable fixed points (saddles), represented by filled circles, in their basin boundaries. In computing these figures, and all attractor-basin portraits hereafter, a fourth-order Runge–Kutta–Gill scheme with fixed step size was used with single precision: initial conditions were chosen on a uniform grid of points, integrations being continued until final behavior was confirmed for each grid point. The integration step sizes and the numbers of grid points are given in each figure caption as well as the values of the system parameters. In Fig. 14, a sequence of successive enlargements of smaller and smaller regions of the xy plane clearly shows the Cantor set structure of the basin boundaries. There is no end to this enlargement sequence, and similar geometric structure continues infinitely. This property of the basin boundary is called self-similar or fractal. The fractal nature of the basin boundary originates from the homoclinic structure of the invariant branches of the saddle, that is, the α-branch which tends toward the non-resonant attractor (not shown in the figure) crosses the ω-branch which tends toward the saddle from the right side. Some of the homoclinic structure is illustrated in Fig. 1(b) of [29], Fig. 6 of [30] and Fig. 4 of [31]. Also omitted from Fig. 14 are extremely narrow basins of a pair of extremely small two-periodic chaotic attractors which were detected inside the blank region; these small attractors exist only in a very narrow range of parameter values. Note that the characteristic property of a fractal basin boundary is that transient behavior started from the boundary is chaotic and consequently the final steady motion becomes indeterminate.

Before presenting the other attractor-basin portraits, we must here explain our symbols for the fixed and periodic points. We use the following symbols: (○) for sink or completely stable fixed point; (●) for saddle or directly unstable fixed point; (■) for saddle or inversely unstable fixed point; ($\times$, $+$) for n-periodic point ($n = 2, 3$).

The periodic points inside the basins are sinks and ones in the basin boundaries are saddles. As was shown in Fig. 8, multiple periodic groups (attractors) are common; periodic points belonging to the same group are marked by the same symbol. However, in order to avoid complexity, basins of different but related periodic points are not always distinguished. The order of successive movement of images under the mapping f_λ among these basins can be easily seen from the corresponding cases in Fig. 8. Figure 15 shows an attractor-basin phase portrait corresponding to the point (c) on the kB chart of Fig. 7, and final motions are the fundamental harmonic and ultrasubharmonics of order 4/3. Figure 16

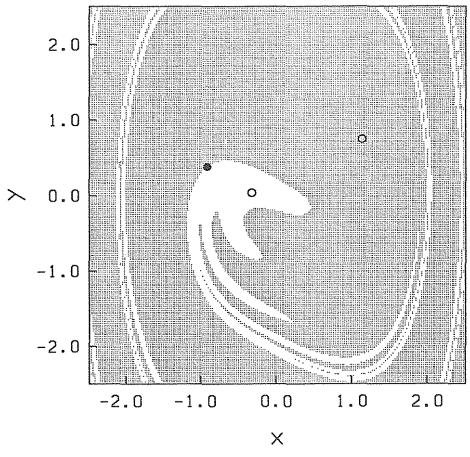

Fig. 13. Attractor-basin phase portrait with integration step size $2\pi/60$ and 201×201 grid of initial conditions for $k = 0.1$, $B = 0.3$. (Reproduced with the courtesy of the European Conference on Circuit Theory and Design [28].)

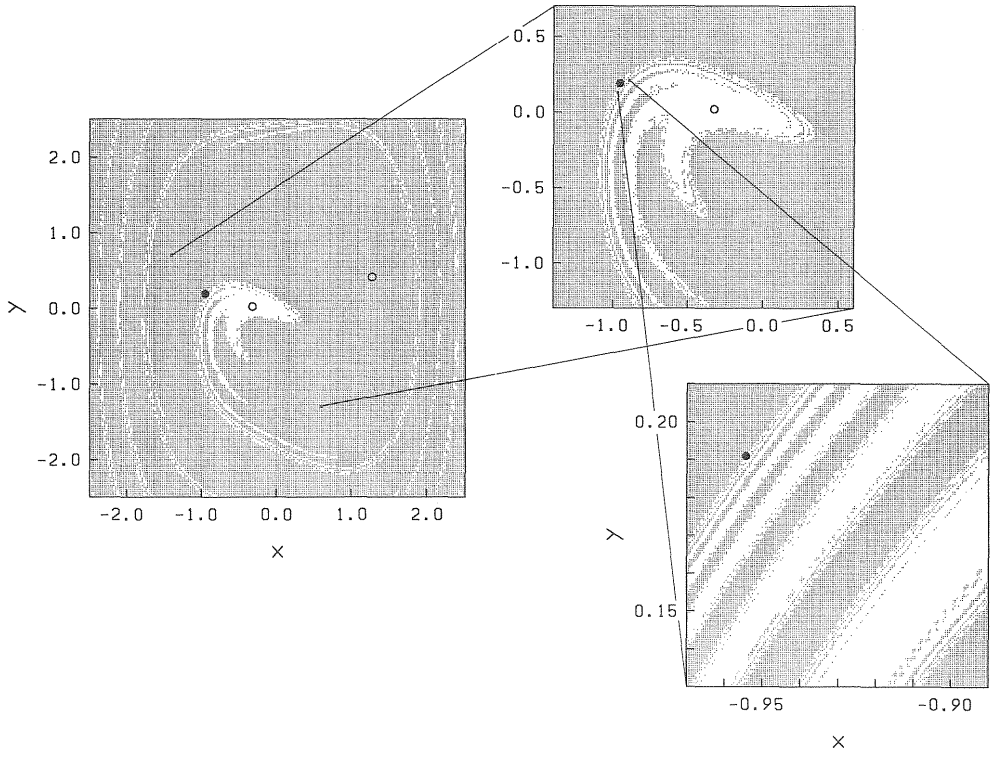

Fig. 14. Attractor-basin phase portrait with integration step size $2\pi/60$ and 201×201, 161×161, 161×161 grid of initial conditions for $k = 0.05$, $B = 0.3$. (Reproduced with the courtesy of the European Conference on Circuit Theory and Design [28].)

corresponds to the point (d), and ultrasubharmonics of order 3/2. Figure 17 corresponds to (e), and ultrasubharmonics of order 5/3. All of these portraits are similar to each other, but it should be noted that for ultrasubharmonics of order m/n, when either m or n is even, there appear a pair of attractors and basins, while in cases where both m and n are odd, only one such attractor appears. This results from the symmetry of the system explained above.

Figure 18 shows an attractor-basin portrait corresponding to the point (j) on the kB chart of Fig. 7; see also [32]. There are two attractors of two-periodic groups; their two basins are separated by the ω-branches of a directly unstable fixed point of f_λ. Furthermore, each basin of a two-periodic point is subdivided by ω-branches of the inversely unstable fixed points. The tails of these four subdivisions of the two basins wind around the two-periodic groups respectively, becoming infinitely thin as they accumulate along the ω-branches of the directly unstable fixed point.

Figure 19 corresponds to the point (n) of Fig. 7. In this example, there exists only one attracting three-periodic group. The three images of this three-periodic point are considered as distinct attractors of the mapping f_λ^3, and the corresponding basins are distinguished. As is seen in the figure, a more complicated configuration appears, that is, each basin of an image of the three-periodic point is bounded by ω-branches of the directly unstable three-periodic points and the tails of these three basins behave in a complicated fashion, seen in the figure, becoming infinitely thin as they accumulate along the ω-branches of the three fixed points (one directly and two inversely unstable saddles). Moreover, tails of the basins are mixed in confusion with each other and accumulate on the ω-branches of these three saddles from both sides. It should be added that a closer inspection reveals that the basin boundaries of Fig. 19 have a fractal structure, but those of Fig. 18 do not. This means that invariant branches of the directly unstable saddles of Fig. 18 are heteroclinic but not homoclinic, while those of Fig. 19 are homoclinic.

Figures 20 and 21 correspond to (q) and (t), respectively. In addition to the completely stable fixed point, there exist two two-periodic groups in Fig. 20 and one three-periodic group in Fig. 21. Below the frame of Fig. 20 there exists a directly unstable fixed point as shown in the figure. Though not indicated in the figure, it has been confirmed that the invariant branches of this saddle have a homoclinic structure. In Fig. 20, the ω-branches delimiting basin boundaries of two-periodic points do not have homoclinic structure, but we have confirmed that these basins are caught in the homoclinic structure of the saddle below the frame, and hence tails of the basins show extremely complicated shape as we see in the figure. This case shows a second mechanism for generating a fractal basin boundary.

Taking the saddle below the frame of Fig. 20 into account, the Levinson–Massera relation (13) concerning the number of the fixed points holds and also equations (14) and (15) can be verified for the n-periodic points $(n = 2, 3)$ for all attractor-basin portraits given above.

Within each region in Fig. 7 identified by Roman numerals, the number of fixed points is constant, but the number changes across the boundaries of these regions. It is believed that all fixed points which can exist within the parameter range of Fig. 7 have been identified, although we cannot exclude the possibility that some fixed points existing in some small region at low damping may have been neglected. From Fig. 8 and the attractor-basin portraits of Figs 13–21 it is conjectured that the counts of fixed points in Table 1 are complete within the indicated regions. Recalling that there are no sources, we use $S(1)$ to denote the number of period one sinks; as before, $D(1)$ and $I(1)$ denote numbers of directly and inversely unstable saddle fixed points.

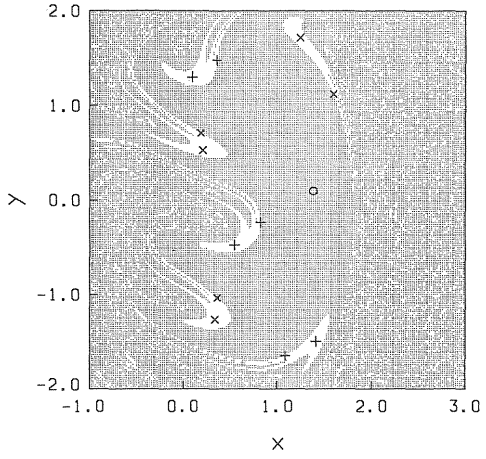

Fig. 15. Attractor-basin phase portrait with integration step size $2\pi/60$ and 201×201 grid of initial conditions for case (c) of Fig. 7; $k = 0.015$, $B = 0.45$. (Reproduced with the courtesy of the European Conference on Circuit Theory and Design [28].)

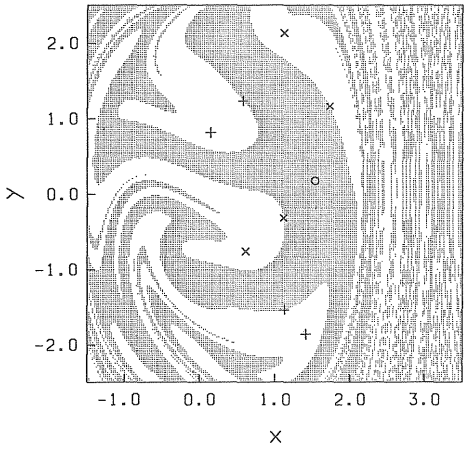

Fig. 16. Attractor-basin phase portrait with integration step size $2\pi/60$ and 201×201 grid of initial conditions for case (d) of Fig. 7; $k = 0.04$, $B = 0.90$. (Reproduced with the courtesy of the European Conference on Circuit Theory and Design [28].)

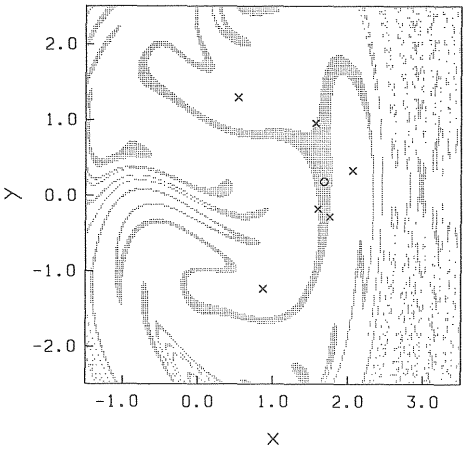

Fig. 17. Attractor-basin phase portrait with integration step size $2\pi/60$ and 201×201 grid of initial conditions for case (e) of Fig. 7; $k = 0.05$, $B = 1.40$. (Reproduced with the courtesy of the European Conference on Circuit Theory and Design [28].)

Table 1. Number of fixed points in the xy plane for various parameter regions

Region in kB chart	Number of fixed points	
I	$S(1) = 2$,	$D(1) = 1$
II–II′–III	$S(1)$ or $I(1) = 2$,	$D(1) = 1$
II′	$S(1) = 4$,	$D(1) = 3$
II ∩ III	$S(1) = 1$,	$S(1)$ or $I(1) = 2$, $D(1) = 2$
III–II	$S(1) = 2$,	$D(1) = 1$
IV	$S(1)$ or $I(1) = 2$,	$D(1) = 1$
Outside I ∪ II ∪ III ∪ IV	$S(1) = 1$	

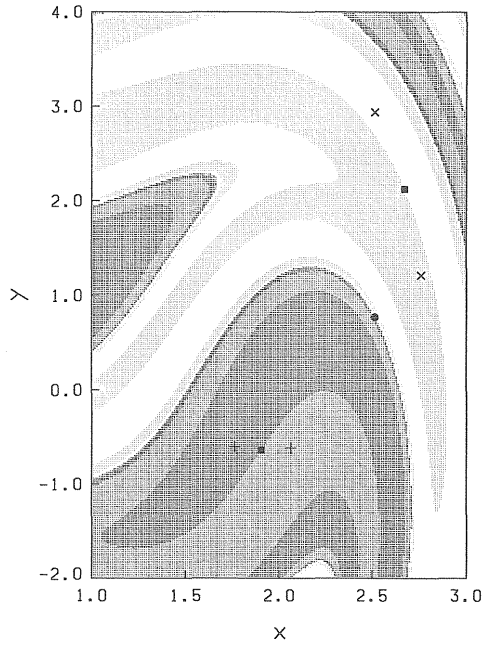

Fig. 18. Attractor-basin phase portrait with integration step size $2\pi/90$ and 201×301 grid of initial conditions for case (j) of Fig. 7; $k = 0.20$, $B = 5.50$. (Reproduced with the courtesy of the European Conference on Circuit Theory and Design [28].)

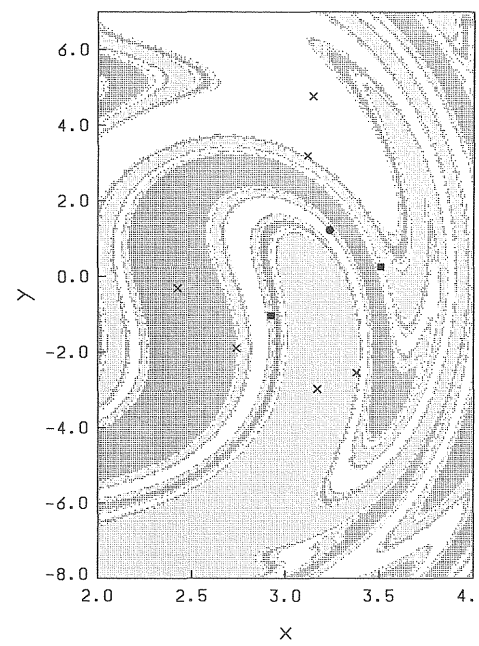

Fig. 19. Attractor-basin phase portrait with integration step size $2\pi/120$ and 201×301 grid of initial conditions for case (n) of Fig. 7; $k = 0.20$, $B = 10.0$. (Reproduced with the courtesy of the European Conference on Circuit Theory and Design [28].)

8. GLOBAL ATTRACTOR STRUCTURE, ATTRACTOR AND BASIN BIFURCATIONS

Let us now interpret the experimental facts described above in light of the theory, particularly the global invariant manifold structures.

Figure 22 shows the chaotic attractor for case (o) in the kB plane, and some of the associated invariant manifold structure. There are three unstable fixed points contained in the attractor, one directly unstable point ${}^1D^1$ and two inversely unstable points ${}^1I^1$ and ${}^2I^1$. The α- and ω-branches of the directly unstable saddle are shown in part, and a number of transverse homoclinic intersections can be seen. As more of these branches are prolonged, self-similar property will appear. Following Birkhoff, this implies the existence of infinitely many periodic points near the homoclinic points.

Numerical evidence strongly suggests that the chaotic attractor is identical with the closure of the α-branches or unstable manifolds of the directly unstable saddle ${}^1D^1$. This phenomenon is not peculiar to the specific parameters of case (o), but occurs for typical parameter values in the corresponding shaded region. The appearance of the attractor seems to vary continuously as the parameter values are changed inside the shaded region near the point (o).

Most homoclinic intersections in Fig. 22 are clearly transverse, but there are a few instances of intersections which are very nearly tangent. It is expected that many such tangencies or near tangencies may appear as more of the invariant manifolds are

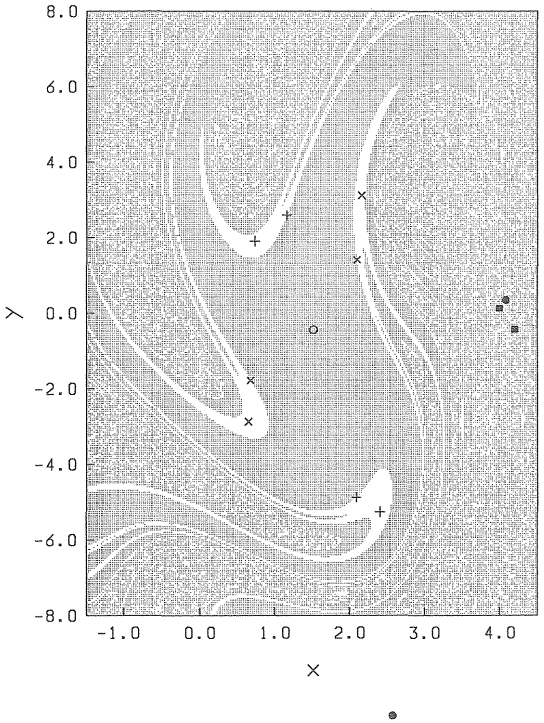

Fig. 20. Attractor-basin phase portrait with integration step size $2\pi/180$ and 241×321 grid of initial conditions for case (q) of Fig. 7; $k = 0.07$, $B = 16.1$. (Reproduced with the courtesy of the European Conference on Circuit Theory and Design [28].)

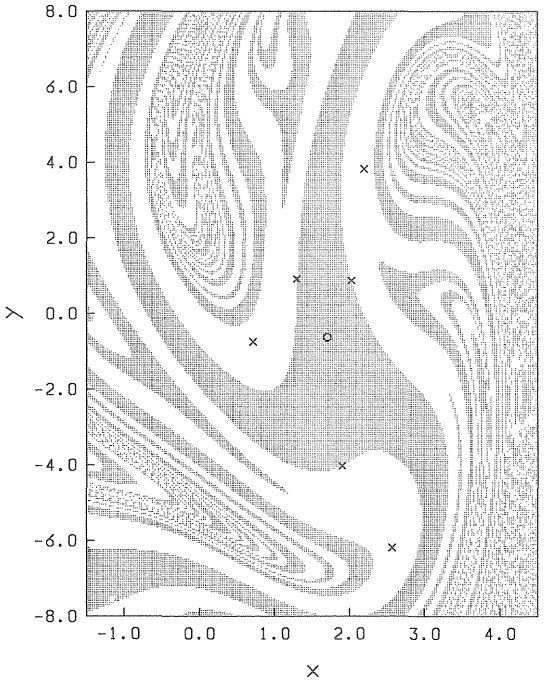

Fig. 21. Attractor-basin phase portrait with integration step size $2\pi/180$ and 241×321 grid of initial conditions for case (t) of Fig. 7; $k = 0.12$, $B = 18.8$. (Reproduced with the courtesy of the European Conference on Circuit Theory and Design [28].)

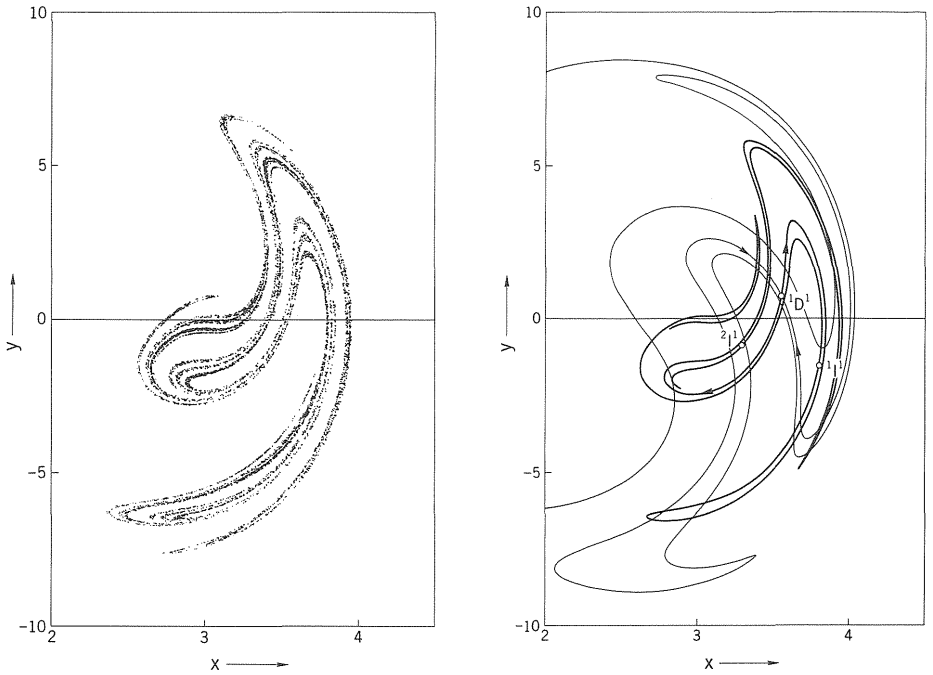

Fig. 22. Chaotic attractor for case (o) and the associated invariant manifold structure. (Reproduced with the courtesy of the Institute of Electrical Engineers of Japan [23].)

constructed. This suggests that the attractor structure may be structurally unstable in the sense of Andronov–Pontryagin.

Numerical experiments show that all of the infinitely many periodic motions in the attractor are unstable. Thus if any sinks exist, their basins of attractions are so small that the smallest amount of noise or error perturbs the system away.

The movement of images in the attractor under iteration is not reproducible, in the sense that nearly identical initial conditions lead eventually to different motions or waveforms. Furthermore, this situation occurs for motions starting from any part of the attractor; this property is referred to as sensitive dependence on initial conditions. On the other hand, any single long-term trajectory will, after transients die away, fill out an apparently identical structure, that is, the closure of the α-branches of $^1D^1$. Thus the numerical evidence strongly suggests that there is a single transitive attractor. A typical orbit returns infinitely often to a neighborhood of any point in the attractor, i.e. there is stability in the sense of Poisson.

Thus the observed motion may be thought of as visiting neighborhoods of various unstable periodic motions, which are infinite in number. The system continues to transit in apparently random manner among the infinitely many unstable periodic solutions. The transit may be influenced by small fluctuations or noise not included in the differential equations but present in the real system or simulation.

For this reason we have called this type of motion a randomly transitional motion [33]. The term chaos has since been widely accepted to describe this type of motion; this term strongly indicates the random aspect of the phenomena, although it may not adequately

convey the very coherent structure which is an equally important aspect of the motion.

Let us now turn to a description of the various routes to chaos observed as the system parameters are varied from outside into the shaded regions. The most commonly observed transition is by successive period doubling, beginning from the two symmetrically related sinks which exist everywhere inside region II. This first period doubling is illustrated in Fig. 8 from case (*i*) to case (*j*). The arc in Fig. 7 passing between points (*i*) and (*j*) shows the location where this first period doubling occurs. Notice that this period doubling bifurcation arc extends over and around to the right side of the shaded regions. A typical path in the kB plane which passes through this arc into the shaded regions leads to chaos via Feigenbaum cascade, generating two symmetrically related chaotic attractors which eventually merge with each other.

A different bifurcation is observed when entering the shaded (*o*) region from the right, that is, from the region typified by case (*p*). At this edge of the shaded (*o*) region, a global bifurcation occurs which causes the chaotic attractor to suddenly appear. The global bifurcation is a homoclinic tangency of the α- and ω-branches of the directly unstable fixed point (filled circle) in the basin boundary. This situation is illustrated in Figs 23–24. The parameter values $k = 0.1$, $B = 13.388$ are the values where the chaotic attractor gains or loses stability, and also the values where the directly unstable fixed point has a homoclinic tangency. This phenomenon was originally described in [34] and called a transition chain; similar phenomena have since been widely reported and are now frequently referred to as boundary crises [35] or blue sky catastrophes [36].

Another example of such a global bifurcation occurs along the right boundary of the shaded region containing case (*l*). Here the chaotic attractor gains or loses stability as it touches a directly unstable three-periodic point, whose α- and ω-branches develop a homoclinic tangency at the bifurcation threshold. This situation is illustrated in Fig. 25.

Note that in both this and the preceding case, the directly unstable point in the basin boundary has no homoclinic structure before the transition chain is established. This means that the chaotic attractor always has a regular basin boundary. In other systems, it can happen that a chaotic attractor exists in a basin with a fractal boundary, that is, homoclinic structure develops in the basin boundary prior to the transition chain or blue sky catastrophe. Further description of this phenomenon can be found in [37], where the term chaotic saddle catastrophe was used; see also [38]. The phenomenon of chaotic saddle catastrophe has not been observed for equation (16) in the region of the kB plane shown in Fig. 7.

Finally we describe the bifurcations passing from the region of case (*n*) to the right into the shaded region typified by case (*o*). Here the phenomena are somewhat more complicated. The chaotic attractor develops from the period three sink of case (*n*). First this period three sink experiences a period doubling cascade which leads to a three-piece chaotic attractor; then there is usually a sudden explosion in size from a three-piece to one large chaotic attractor. Similar phenomena were reported in [39], and have since become widely known as interior crises [35]; see also [13].

We note that in all cases where chaotic attractors are observed, they contain among the periodic points of lowest period either one inversely unstable point, or one directly unstable and two inversely unstable points. Recently Stewart has conjectured that this can be explained by applying the Levinson–Massera index equations to an appropriate subregion of the xy plane [40].

Sometimes the global structure of the phase portrait may have important consequences even though all attractors are regular periodic motions. For example, a local saddle-node or fold bifurcation causes the system to undergo a rapid transient to some other attractor; and it can happen that if two or more attractors are available, the one chosen may depend

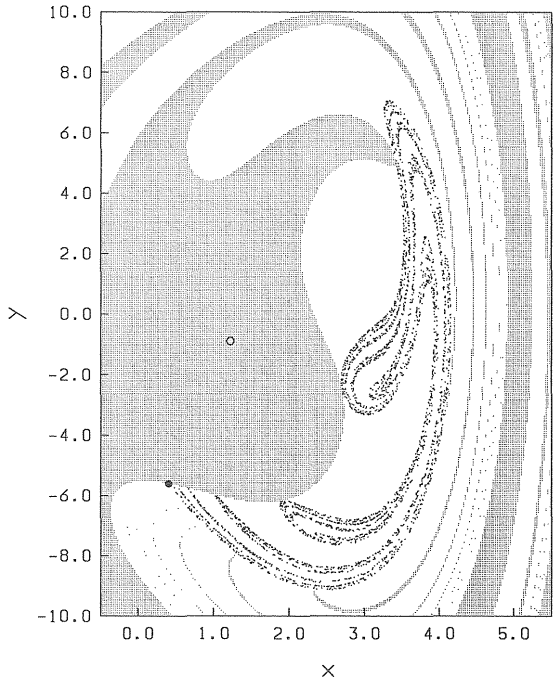

Fig. 23. Attractor-basin phase portrait with integration step size $2\pi/180$ and 241×321 grid of initial conditions for $k = 0.1$, $B = 13.388$.

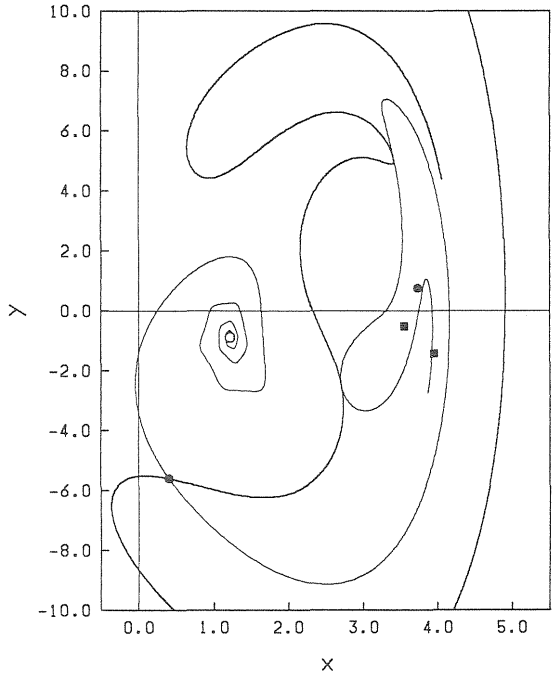

Fig. 24. Invariant manifold structure showing homoclinic tangency corresponding to Fig. 23.

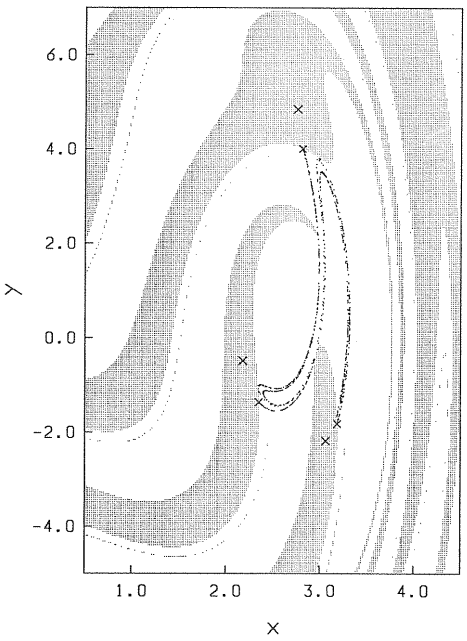

Fig. 25. Attractor-basin phase portrait with integration step size $2\pi/120$ and 201×301 grid of initial conditions for $k = 0.25$, $B = 8.812$.

very sensitively on how the bifurcation is realized in the simulation or real-world system. Such indeterminate bifurcations can be observed in the Duffing equation (16), for example by crossing the boundary of region I in the kB plane. Although the bifurcation event is local, the outcome is determined by global structure: the probabilities of settling on the various attractors available can be estimated from the structure of invariant manifolds; see [41].

9. CONCLUSION

By summarizing the author's previous reports [23–24, 28, 33–34, 39], regular and chaotic phenomena have been surveyed which occur in the system governed by the Duffing equation. The global attractor structure, and attractor and basin bifurcations have been discussed in relation to the geometric theory of differential equations. Chaotic attractors have been observed over a wide range of parameter values. Multiple coexisting attractors are also common; both regular and fractal basin boundaries are observed. The structure of chaotic attractors, basin boundaries and bifurcations have been understood in terms of unstable periodic motions and invariant manifolds.

High resolution portraits of chaotic attractors shown in Fig. 9(k) and (o_1) were lucky enough to earn the attention of a wide audience: D. Ruelle named the attractor of Fig. 9(o_1) *Japanese attractor* [5, 6], and Thompson and Steward referred to the attractor of Fig. 9(k) as *Ueda's chaotic attractor* [2]. Ueda's chaotic attractor shown in Fig. 26 and the Japanese attractor in Fig. 27 conclude the article. Both pictures are depicted taking the unit length of the x-axis to be five times that of the y-axis, and 100,000 steady state points are plotted.

Acknowledgement—I owe sincere thanks to the mathematician Dr Hugh Bruce Stewart of the Division of Applied Science, Brookhaven National Laboratory, for his generous assistance in preparing this article. Not only did he graciously agree to edit my manuscript, which was written in poor English, but he also provided me with much valuable advice in structuring the text as well as selecting the figures. I would like to point out that most of the items within the text that are not specifically described in the References [23–24, 28, 33–34, 39], are largely a result of his advice.

I would also like to thank Dr Stewart as well as Professor Ralph Abraham of the University of California Santa Cruz, especially for their insight into the significance of C. Pugh's closing lemma, which I had not fully grasped.

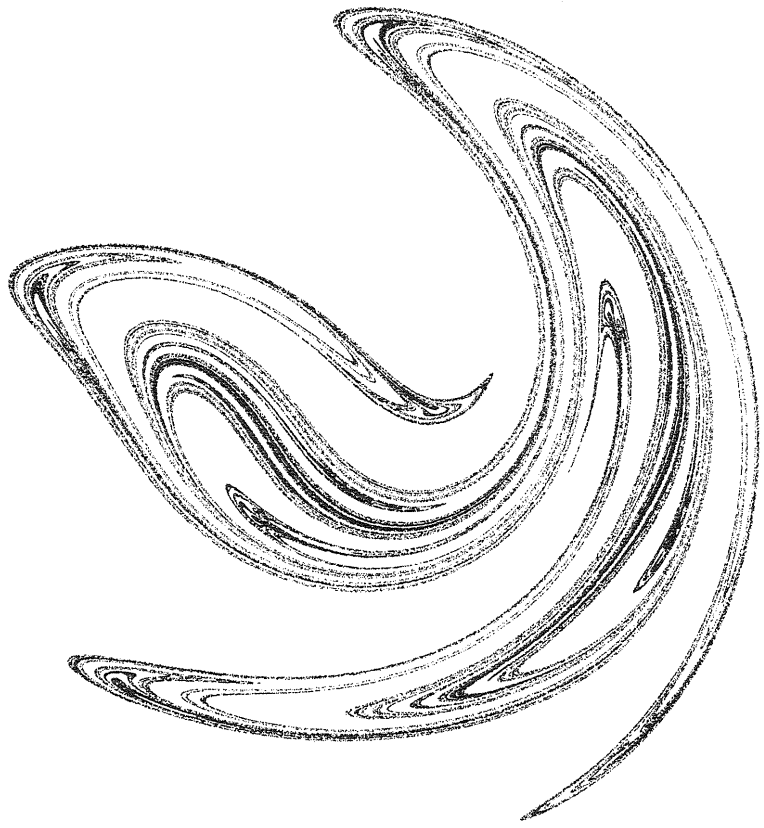

Fig. 26. Ueda's chaotic attractor.

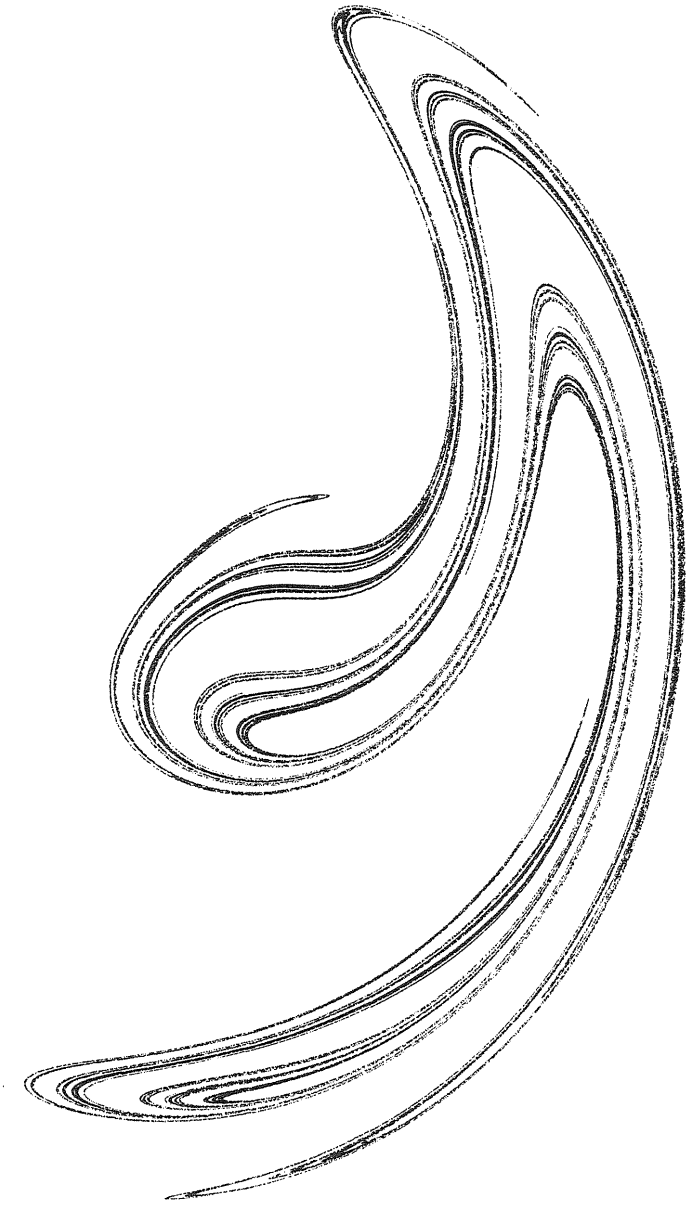

Fig. 27. Japanese attractor.

REFERENCES

1. G. Duffing, *Erzwungene Schwingungen bei veränderlicher Eigenfrequenz und ihre technische Bedeutung*. Vieweg, Braunschweig (1918).
2. J. M. T. Thompson and H. B. Stewart, *Nonlinear Dynamics and Chaos*. Wiley, New York (1986).
3. D. Ruelle and F. Takens, On the nature of turbulence, *Commun. Math. Phys.* **20**, 167–192; **23**, 343–344 (1971).
4. C. Hayashi, Y. Ueda, N. Akamatsu and H. Itakura, On the behavior of self-oscillatory systems with external forcing. *Trans. Inst. Commun. Engrs* **53A**, 150–158 (1970) (in Japanese); English Translation, *Electronics and Communications in Japan*, pp. 31–39. Scripta, Silver Spring, MD.
5. D. Ruelle, Les attracteurs étranges, *La Recherche* **11**, 132–144 (1980).
6. D. Ruelle, Strange attractors, *The Mathematical Intelligencer* **2**, 126–137 (1980).
7. H. Poincaré, *Les Méthodes Nouvelles de la Mécanique Céleste*, Vols 1–3. Gauthier-Villars, Paris (1899).
8. G. D. Birkhoff, *Collected Mathematical Papers*. American Mathematical Society, Providence, RI (1950); Republication, Dover Publications, New York (1968).
9. E. A. Coddington and N. Levinson, *Theory of Ordinary Differential Equations*. McGraw-Hill, New York (1955).
10. V. V. Nemytskii and V. V. Stepanov, *Qualitative Theory of Differential Equations*. Princeton University Press, Princeton, NJ (1960).
11. R. Abraham, *Foundations of Mechanics*. Benjamin, New York (1967).
12. R. Abraham and J. E. Marsden, *Foundations of Mechanics*. Benjamin/Cummings, Massachusetts (1978).
13. R. H. Abraham and C. D. Shaw, *Dynamics: The Geometry of Behavior, Part One, Periodic Behavior* (1982); *Part Two, Chaotic Behavior* (1983); *Part Three, Global Behavior* (1985); *Part Four, Bifurcation Behavior* (1988). Aerial Press, Santa Cruz, CA.
14. J. Guckenheimer and P. Holmes, *Nonlinear Oscillations, Dynamical Systems, and Bifurcations of Vector Fields*. Springer, New York (1983).
15. F. C. Moon, *Chaotic Vibrations, An Introduction for Applied Scientists and Engineers*. Wiley, New York (1987).
16. D. K. Arrowsmith and C. M. Place, *An Introduction to Dynamical Systems*. Cambridge University Press, Cambridge (1990).
17. N. Levinson, Transformation theory of non-linear differential equations of the second order, *Ann. Math.* **45**, 723–737 (1944); *Correction* **49**, 738 (1948).
18. N. Levinson, On the existence of periodic solutions for second order differential equations with a forcing term, *J. Math. Phys.* **22**, 41–48 (1943).
19. N. Levinson, On a non-linear differential equation of the second order, *J. Math. Phys.* **22**, 181–187 (1943).
20. C. C. Pugh, An improved closing lemma and a general density theorem, *Am. J. Math.* **89**, 1010–1021 (1967).
21. J. L. Massera, The number of subharmonic solutions of non-linear differential equations of the second order, *Ann. Math.* **50**, 118–126 (1949).
22. E. C. Zeeman, Bifurcation and catastrophe theory, in *Contemporary Mathematics*, Vol. 9, pp. 207–272. American Mathematical Society, Providence, RI (1982).
23. Y. Ueda, Random phenomena resulting from nonlinearity, *Trans. Inst. Electrical Engrs* **98A**, 167–173 (1978) (in Japanese); English Translation, *Int. J. Non-Linear Mech.* **20**, 481–491 (1985).
24. Y. Ueda, Steady motions exhibited by Duffing's equation: a picture book of regular and chaotic motions, in *New Approaches to Nonlinear Problems in Dynamics*, edited by P. J. Holmes, pp. 311–322. SIAM, Philadelphia (1980).
25. C. Hayashi, *Forced Oscillations in Non-Linear Systems*. Nippon Printing and Publishing Co., Osaka, Japan (1953).
26. C. Hayashi, *Nonlinear Oscillations in Physical Systems*. McGraw-Hill, New York (1964).
27. C. Hayashi, *Selected Papers on Nonlinear Oscillations*. Nippon Printing and Publishing Co., Osaka, Japan (1975).
28. Y. Ueda and S. Yoshida, Attractor-basin phase portraits of the forced Duffing's oscillator, *Proc. European Conf. Circuit Theory Design*, Paris, Vol. 1, pp. 281–286 (1987).
29. C. Hayashi, Y. Ueda and H. Kawakami, Transformation theory as applied to the solutions of non-linear differential equations of the second order, *Int. J. Non-Linear Mech.* **4**, 235–255 (1969).
30. C. Hayashi, Y. Ueda and H. Kawakami, Periodic solutions of Duffing's equation with reference to doubly asymptotic solutions, *Proc. 5th Int. Conf. Nonlinear Oscillations*, Kiev, Vol. 2, pp. 507–521 (1970).
31. C. Hayashi and Y. Ueda, Behavior of solutions for certain types of nonlinear differential equations of the second order, *Proc. 5th Int. Conf. Nonlinear Oscillations*, Poznań, Vol. 14, pp. 341–351 (1973).
32. C. Hayashi, Y. Ueda and H. Kawakami, Solution of Duffing's equation using mapping concepts, *Proc. 4th Int. Conf. Nonlinear Oscillations*, Prague, pp. 25–40 (1968).
33. Y. Ueda, N. Akamatsu and C. Hayashi, Computer simulation of nonlinear ordinary differential equations and non-periodic oscillations, *Trans. Inst. Commun. Engrs* **56A**, 218–225 (1973) (in Japanese); English Translation, *Electronics and Communications in Japan*, pp. 27–34. Scripta, Silver Spring, MD.
34. Y. Ueda, Randomly transitional phenomena in the system governed by Duffing's equation, *J. Statistical Phys.* **20**, 181–196 (1979).

35. C. Grebogi, E. Ott and J. A. Yorke, Crises, sudden changes in chaotic attractors, and transient chaos, *Physica* **7D**, 181–200 (1983).
36. R. H. Abraham, Chaostrophes, intermittency, and noise, in *Chaos, Fractals, and Dynamics*, edited by P. Fischer and W. R. Smith, pp. 3–22. Marcel Dekker, New York (1985).
37. H. B. Stewart, A chaotic saddle catastrophe in forced oscillators, in *Dynamical Systems Approaches to Nonlinear Problems in Systems and Circuits*, edited by F. M. A. Salam and M. L. Levi, pp. 138–149. SIAM, Philadelphia (1988).
38. C. Grebogi, E. Ott and J. A. Yorke, Basin boundary metamorphoses: changes in accessible boundary orbits, *Physica* **24D**, 243–262 (1987).
39. Y. Ueda, Explosion of strange attractors exhibited by Duffing's equation, *Ann. NY Acad. Sci.* **357**, 422–434 (1980).
40. H. B. Stewart, Application of fixed point theory to chaotic attractors of forced oscillators, Research Report, NIFS-62, National Institute for Fusion Science, Nagoya, Japan (1990); *Japan J. Ind. Appl. Math.*, to appear.
41. H. B. Stewart and Y. Ueda, Catastrophes with indeterminate outcome, *Proc. R. Soc.* **A432**, 113–123 (1991).